



ARTICLE

# PDGFR $\beta$ translocates to the nucleus and regulates chromatin remodeling via TATA element–modifying factor 1

Natalia Papadopoulos<sup>1,2</sup> , Johan Lennartsson<sup>2,3</sup>, and Carl-Henrik Heldin<sup>1,2</sup> 

Translocation of full-length or fragments of receptors to the nucleus has been reported for several tyrosine kinase receptors. In this paper, we show that a fraction of full-length cell surface platelet-derived growth factor (PDGF) receptor  $\beta$  (PDGFR $\beta$ ) accumulates in the nucleus at the chromatin and the nuclear matrix after ligand stimulation. Nuclear translocation of PDGFR $\beta$  was dependent on PDGF-BB–induced receptor dimerization, clathrin-mediated endocytosis,  $\beta$ -importin, and intact Golgi, occurring in both normal and cancer cells. In the nucleus, PDGFR $\beta$  formed ligand-inducible complexes with the tyrosine kinase Fer and its substrate, TATA element–modifying factor 1 (TMF-1). PDGF-BB stimulation decreased TMF-1 binding to the transcriptional regulator Brahma-related gene 1 (Brg-1) and released Brg-1 from the SWI–SNF chromatin remodeling complex. Moreover, knockdown of TMF-1 by small interfering RNA decreased nuclear translocation of PDGFR $\beta$  and caused significant up-regulation of the Brg-1/p53-regulated cell cycle inhibitor *CDKN1A* (encoding p21) without affecting PDGFR $\beta$ -inducible immediate-early genes. In conclusion, nuclear interactions of PDGFR $\beta$  control proliferation by chromatin remodeling and regulation of p21 levels.

## Introduction

PDGF family members stimulate mitogenesis and chemotaxis of fibroblasts, pericytes, and smooth muscle cells (Heldin and Westermark, 1999) and exert their effects via binding to  $\alpha$ - and  $\beta$ -tyrosine kinase receptors (PDGFR $\alpha$  and PDGFR $\beta$ , respectively). Binding of ligands to the extracellular domains of PDGF receptors (PDGFRs) triggers dimerization of the receptors and autophosphorylation within their intracellular domains, leading to activation of multiple signaling pathways; their signaling is disrupted in various pathological conditions, including cancer (Papadopoulos and Lennartsson, 2017; Heldin et al., 2018). PDGFRs are internalized from the plasma membrane via receptor-mediated endocytosis (Lemmon and Schlessinger, 2010) and continue to assemble signaling complexes and transmit signals while internalized in endosomes (Miaczynska et al., 2004; Miaczynska, 2013). Notably, internalized growth factor receptors may activate different signaling molecules depending on their various intracellular localizations (Schlessinger and Lemmon, 2006; Kermorgant and Parker, 2008; Sigismund et al., 2008; Choudhary et al., 2009). Moreover, there is increasing evidence suggesting that membrane receptors not only signal from the plasma membrane and intracellular vesicles, but are able to

traffic to the nucleus in a ligand-dependent manner and transmit signals by direct binding to DNA and/or by participating in other nuclear events (Carpenter and Liao, 2013). Among prominent examples are EGF receptor (EGFR) family members (Lo et al., 2006; Wang et al., 2010a, 2012; De Angelis Campos et al., 2011) and insulin growth factor receptor 1 (IGF-1R; Aleksic et al., 2010; Packham et al., 2015).

Nuclear receptor tyrosine kinases (RTKs) have been found to transactivate promoters of target genes (Lin et al., 2001), interact with transcription factors (Wang et al., 2010b), affect DNA replication and damage repair (Wang et al., 2006), bind to putative enhancer elements on genomic DNA (Sehat et al., 2010), and regulate transcription of ribosomal RNA genes independently of canonical activation of downstream phosphatidylinositol-3-kinase (PI3-kinase) and Erk MAP-kinase pathways (Li et al., 2011). Recently, IGF-1R was shown to phosphorylate histone H3 on tyrosine 41, leading to stabilization of the Brahma-related gene (Brg-1) chromatin binding (Warsito et al., 2016).

In the nucleus, genomic DNA is packaged into nucleosomes that are organized in higher order chromatin structures forming functional compartments and chromosomal territories of active

<sup>1</sup>Science for Life Laboratory, Department of Medical Biochemistry and Microbiology, Uppsala University, Uppsala, Sweden; <sup>2</sup>Science for Life Laboratory, Ludwig Institute for Cancer Research, Uppsala University, Uppsala, Sweden; <sup>3</sup>Department of Pharmaceutical Biomedicine, Uppsala University, Uppsala, Sweden.

Correspondence to Carl-Henrik Heldin: [c-h.heldin@imbim.uu.se](mailto:c-h.heldin@imbim.uu.se).

© 2018 Papadopoulos et al. This article is distributed under the terms of an Attribution–Noncommercial–Share Alike–No Mirror Sites license for the first six months after the publication date (see <http://www.rupress.org/terms/>). After six months it is available under a Creative Commons License (Attribution–Noncommercial–Share Alike 4.0 International license, as described at <https://creativecommons.org/licenses/by-nc-sa/4.0/>).

and repressed chromatin (Strouboulis and Wolffe, 1996). It has been shown that transcriptionally active DNA is tightly associated with the nuclear skeleton (or nuclear matrix), whereas inactive loci are not (Jackson et al., 1993). The SWI-SNF chromatin remodeling complex is enriched at the active chromatin and associated with the nuclear matrix (Reyes et al., 1997). It is a large protein complex that provides coordinate regulation of gene expression programs. The SWI-SNF complex consists of multiple subunits, including mutually exclusive DNA helicase ATPases Brahma homologue (BRM) and Brg-1, "core" elements Brg-1-associated factors 155 and 170 (BAF155 and BAF170), and variable modulatory subunits (Wilson and Roberts, 2011). SWI-SNF chromatin remodeling complexes were found to act as tumor suppressors; their subunit proteins are deleted or mutated in ~20% of human cancers, exhibiting a broad mutation pattern similar to that of TP53 (Kadoch et al., 2013). Interestingly, activation of T lymphocytes with phosphatidylinositol 4,5-bisphosphate led to rapid changes in chromatin binding of SWI-SNF complexes, thus demonstrating a direct interface between signaling at the membrane and chromatin regulation (Zhao et al., 1998; Rando et al., 2002).

TATA element-modifying factor 1 (TMF-1), also named androgen receptor activator 160 kD (ARA160), is a Golgi protein that mediates intracellular transport by tethering vesicles (Fridmann-Sirkis et al., 2004; Yamane et al., 2007). In the nucleus, TMF-1 competes with TATA-binding protein for binding to some RNA polymerase II TATA box-containing promoters (Garcia et al., 1992), serves as a coactivator of the androgen receptor in human prostate cells (Hsiao and Chang, 1999), and has been copurified with the SWI-SNF chromatin remodeling complex (Euskirchen et al., 2011). TMF-1 can be tyrosine phosphorylated by the nuclear nonreceptor tyrosine kinase Fer (Schwartz et al., 1998), which we previously reported to interact with PDGFR $\beta$  and to play a critical role in PDGF-BB-induced STAT3 activation and cell transformation (Lennartsson et al., 2013).

Here, we show that PDGFR $\beta$  rapidly translocates to the nucleus and localizes to the chromatin and nuclear matrix in response to PDGF-BB stimulation in human BJhTERT fibroblasts and other cell lines. Nuclear interaction of PDGFR $\beta$  with nonreceptor tyrosine kinase Fer and TMF-1 leads to reassembly of Brg-1-containing SWI-SNF complexes, subsequent chromatin remodeling, and changes in the expression of *CDKN1A* mRNA and its encoded protein p21, affecting regulation of cell proliferation.

## Results

### PDGF stimulation causes nuclear accumulation of full-length PDGFR $\beta$

To explore whether PDGFR $\beta$  is translocated to the nucleus, we isolated nuclei and found that in response to PDGF-BB stimulation, there was an accumulation of PDGFR $\beta$  in the nucleus in a time-dependent manner (Fig. 1, a and b). Nuclei of unstimulated cells contained a basic level of PDGFR $\beta$ , calculated as 7% relative to the total amount of the receptor in the cells. The observed nuclear accumulation was increased already after 5 min of PDGF-BB stimulation, reached a peak of 26% of the total receptor amount at 30 min, and then gradually declined, returning to

baseline after ~2 h of PDGF-BB stimulation. The decrease was concomitant with a decrease in cytoplasmic levels of PDGFR $\beta$  during the course of stimulation (Fig. 1 b), reflecting subsequent degradation of PDGFR $\beta$ . Based on the migration properties in an SDS-PAGE gel, as well as using different antibodies recognizing either the extracellular or intracellular regions of the PDGFR $\beta$ , we concluded that the full-length receptor enters the nucleus. Immunoblotting with a phosphotyrosine antibody (Fig. 1 c) revealed that the nuclear PDGFR $\beta$  was phosphorylated. To exclude the possibility that nuclei were contaminated with cytoplasmic organelles, we optimized our protocol and analyzed nuclear extracts (using lamin A/C as the nuclear marker) for purity from plasma membrane (using CD49b as a marker), lipid rafts (marker caveolin), Golgi (marker GM130), ER (marker Bip/GRP78), soluble cytoplasm (marker tubulin), lysosomes (marker Lamp-1), and early endosomes (marker EEA1; Fig. S1).

We confirmed the presence of PDGFR $\beta$  in the nucleus by confocal microscopy of immunofluorescent staining with antibodies raised against the intracellular (Fig. S2 a) and extracellular (Fig. S2 c), parts of PDGFR $\beta$ , as well as by costaining with these antibodies (Fig. 1 d). After PDGF-BB stimulation, PDGFR $\beta$  (Fig. S2, in red) stained as punctuate, dot-like structures both in the cytoplasm and in the nucleus (also see magnification of the nuclear area), presumably as a consequence of dimerization and clustering of the receptor molecules. We performed Z stacks through the nucleus (Fig. S2 b), which confirmed the presence of PDGFR $\beta$  in the middle of the nucleus. Additionally, we performed stacks through the nucleus of the cells costained with two PDGFR $\beta$  antibodies, thus demonstrating localization in the middle of the nucleus for the fraction of PDGFR $\beta$  that was recognized by both antibodies (Fig. 1 d). To further confirm our findings, we performed double staining of PDGFR $\beta$  with an antibody against the total receptor and a phosphotyrosine antibody, detecting autophosphorylated PDGFR $\beta$ . Analysis of images showed colocalization of the signals and the presence of phosphorylated PDGFR $\beta$  in the nucleus (Fig. 1 e). Altogether, these findings indicate that the full-length PDGFR $\beta$  translocates to the nucleus in response to PDGF-BB stimulation.

### PDGFR $\beta$ kinase activity promotes, but is not necessary for, PDGFR $\beta$ nuclear accumulation

To determine whether the kinase activity of PDGFR $\beta$  is required for the nuclear translocation, we used the PDGFR kinase inhibitor AG1296. Although AG1296 treatment resulted in reduced nuclear translocation by ~50%, PDGFR $\beta$  still appeared in the nucleus after PDGF-BB stimulation (Fig. 2, a and b). Similar results were obtained by the unrelated PDGFR kinase inhibitor imatinib (not depicted). Most probably, the reduction in the nuclear translocation of PDGFR $\beta$  reflects the decrease in internalization of the cell surface receptor after inhibition of its kinase activity (Sorkin et al., 1991). To further understand the translocation mechanism, we treated cells with the general phosphatase inhibitor sodium pervanadate, which induces strong receptor phosphorylation in the absence of ligand-induced receptor dimerization. Despite achieving PDGFR $\beta$  phosphorylation, as determined by a phospho-specific PDGFR $\beta$  antibody, P857 (Fig. 2 c, bottom), pervanadate treatment was not sufficient to provoke nuclear

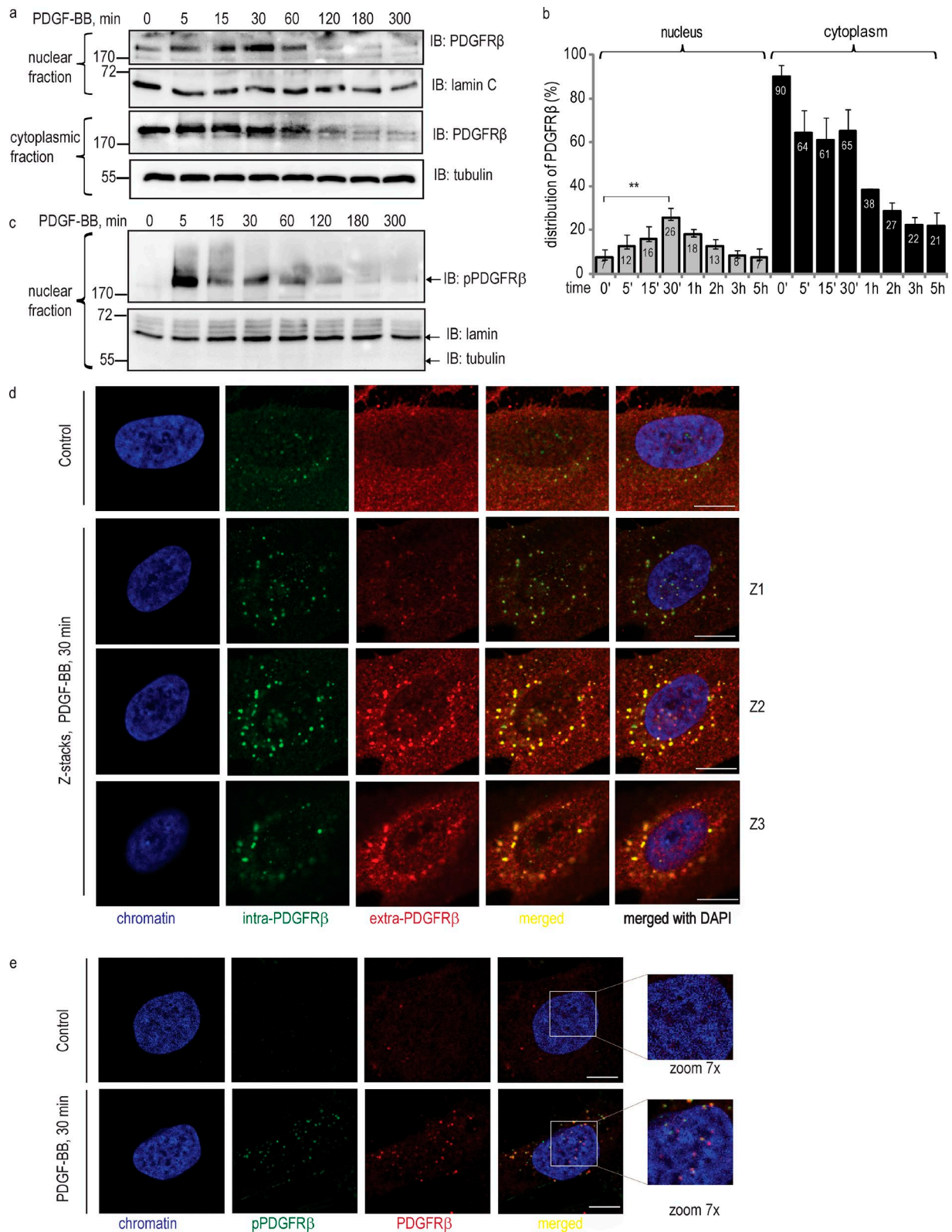


Figure 1. **Nuclear translocation of PDGFRβ in response to ligand stimulation.** (a) Immunoblotting analysis of nuclear and cytoplasmic distribution of PDGFRβ. Nuclear and cytoplasmic fractions were immunoblotted for total PDGFRβ, showing nuclear accumulation of PDGFRβ (top) versus cytoplasmic localization (bottom). Lamin A/C and tubulin were used as markers for nuclear and cytoplasmic fractions, respectively. (b) The distribution of PDGFRβ in the nucleus and in the cytoplasm was quantified as emission values of the immunoblot signal, normalized to the signal of the markers. Total amount of receptor in the cell was calculated as the sum of signal intensity values detected in nuclear and cytoplasmic fractions before stimulation with PDGF-BB (0 min), which was taken as 100%. The signal values obtained during the course of stimulation were calculated relative to this value. Error bars indicate SD. Quantification was based on



translocation (Fig. 2 c, top), suggesting that ligand-induced dimerization of PDGFR $\beta$ , but not receptor phosphorylation, is necessary for nuclear translocation.

### Characterization of the nuclear translocation pathway

Internalization of PDGFR $\beta$  leads to its subsequent degradation via proteasomal (Mori et al., 1992) and lysosomal (Haglund et al., 2003) pathways. We investigated whether inhibition of degradation affected the nuclear accumulation of PDGFR $\beta$ . Interestingly, lysosomal inhibition by chloroquine (Fig. 3 a) resulted in selective nuclear accumulation of PDGFR $\beta$ , whereas proteasomal inhibition by MG132 led to a concomitant increase in PDGFR $\beta$  levels in the cytoplasm and the nucleus (Fig. 3 b). This suggests that the sorting pathways of PDGFR toward the nucleus prevent lysosomal degradation of PDGFR $\beta$ , whereas proteasomal degradation occurs ubiquitously in both the cytoplasm and the nucleus.

To determine whether the receptors seen in the nucleus represented either receptors internalized from the cell surface or newly synthesized receptors, we biotinylated cell surface proteins before PDGF-BB treatment and analyzed the presence of biotinylated PDGFR $\beta$  in the nuclear fraction. Indeed, we detected an accumulation of biotinylated, plasma membrane-derived PDGFR $\beta$  in the nucleus (Fig. 3 c, top) with comparable kinetics as observed for the unlabeled PDGFR $\beta$  (Fig. 3 d). As a negative control, we used the transferrin receptor, which is a transmembrane protein that does not respond to PDGF-BB stimulation; this receptor was not translocated to the nucleus (Fig. 3 c, bottom).

We proceeded to block common subcellular trafficking pathways that are known to be involved in sorting RTKs. PDGFR $\beta$  internalizes from the cell surface to a large extent through clathrin-coated pits (Kapeller et al., 1993) and to some extent through lipid rafts via caveolae-containing vesicles (Liu et al., 1996). Indeed, depletion of cells of clathrin with siRNA efficiently blocked nuclear PDGFR $\beta$  accumulation after PDGF-BB stimulation (Fig. 3 e), supporting the notion that the cell surface PDGFR $\beta$  is sorted toward the nucleus via clathrin-coated vesicles.

Interaction with  $\beta$ -importin is required by many proteins for their entry into the nucleus. We found that when  $\beta$ -importin levels were down-regulated by 85% by siRNA, there was a significant inhibition of nuclear PDGFR $\beta$  accumulation (Fig. 3, f and g), suggesting that translocation of PDGFR $\beta$  to the nucleus occurs in a  $\beta$ -importin-dependent manner.

Recently, it has been proposed that EGFR accumulates in the nucleus by using the retrograde transport machinery from Golgi to the ER. We investigated the importance of Golgi for the nuclear transport of PDGFR $\beta$  by inhibiting all trans-Golgi trafficking with brefeldin A (Fig. 4, a–c) and redistributing the

Golgi complex to the ER with ADP ribosylation factor 1 (Arf-1) siRNA (Fig. 4, d–f). In both cases, we observed some reduction in the nuclear accumulation of PDGFR $\beta$ , and cytoplasmic levels of mature PDGFR $\beta$  were also decreased. Because we found an interaction between PDGFR $\beta$  and TMF-1 in the nucleus (see below), and because TMF-1 was reported to play an important role in intra-Golgi trafficking (Wong and Munro, 2014) and in the retrograde transport from Golgi to ER (Yamane et al., 2007), we investigated whether TMF-1 is necessary for the nuclear translocation of PDGFR $\beta$ . Indeed, when BJhTERT fibroblasts were depleted of TMF-1 with siRNA, a certain decrease of nuclear accumulation of PDGFR $\beta$  at 30 min of PDGF-BB stimulation was observed (Fig. 4, g and h). The cytoplasmic levels of PDGFR $\beta$  were also affected, which suggests that TMF-1 is involved in maintaining cytoplasmic levels of PDGFR $\beta$  as well as participating in its nuclear function.

To further clarify the involvement of TMF-1-positive Golgi vesicles in the nuclear transport of PDGFR $\beta$ , we biotinylated cell surface PDGFR $\beta$  and investigated triple colocalization between biotin, PDGFR $\beta$ , and TMF-1, thus detecting biotinylated cell surface-derived PDGFR $\beta$  interacting with TMF-1 in the area of Golgi and in the nucleus (Fig. 5). After quantification of colocalization (Fig. 5 k), we detected on average 13 biotinylated PDGFR $\beta$  clusters per cell ( $n = 29$ ) within Golgi and 14 within the nucleus after 30 min of stimulation with mean Pearson coefficients of  $0.6 \pm 0.19$  and  $0.35 \pm 0.36$ , respectively. A Pearson coefficient  $>0$  indicates probability of colocalization. Although most biotinylated PDGFR $\beta$  clusters positively correlated with TMF-1, on average 2.5 dots per cell in the Golgi and 2.4 dots per cell in the nucleus displayed triple positive correlation with a Pearson coefficient  $>0.2$ . These findings suggest that biotinylated PDGFR $\beta$  traffics to the nucleus via TMF-1-positive Golgi vesicles.

### Nuclear translocation of PDGFR $\beta$ occurs in both normal and cancer cells

To assess the generality of translocation of PDGFR $\beta$ , we analyzed several different cell lines expressing endogenous PDGFR $\beta$ , such as primary fibroblasts AG1523 (Fig. S3 a), glioblastoma U105MG (Fig. S3 b), and osteosarcoma U2OS (Fig. S3 c) cells. We found that nuclear translocation of PDGFR $\beta$  occurred in both normal and cancer cells. The effect of the receptor kinase inhibitor AG1296 on primary fibroblasts and on glioblastoma and osteosarcoma cancer cell lines was similar to that observed in BJhTERT fibroblasts, i.e., nuclear translocation of PDGFR $\beta$  was decreased, but not completely blocked. In the same way, the effects of brefeldin and MG132 were reproduced in the osteosarcoma cell line U2OS (Fig. S3 c).

three independent experiments, and *t* test statistical analysis was performed for the difference between PDGFR $\beta$  signal in unstimulated nuclei and at 30 min of stimulation with PDGF-BB; \*\*,  $P = 0.0092$ . (c) Immunoblotting of nuclear fractions using a phosphotyrosine antibody, detecting phosphorylated PDGFR $\beta$  (top). The purity of the fractionation was verified (bottom). (d) Nuclear localization of PDGFR $\beta$  as detected by costaining with two types of PDGFR $\beta$  antibodies. PDGFR $\beta$  was stained with intra-PDGFR $\beta$  antibody (green) and with extra-PDGFR $\beta$  antibody (red); chromatin was stained with DAPI (blue). Merged images are shown with (red, green, and blue) and without the nucleus (red and green). Z1, Z2, and Z3 rows of images show stacks through the nucleus of cells stimulated with PDGF-BB for 30 min. Bars, 10  $\mu$ m. (e) Colocalization of immunostaining for total and phospho-specific PDGFR $\beta$  antibodies. Cells were immunostained with total PDGFR $\beta$  antibody (red) and pTyr (PY99) antibody (green); chromatin was stained with DAPI (blue). Images were taken with the focus on the nucleus; yellow indicates colocalization. Molecular mass was measured in kilodaltons. Bars, 10  $\mu$ m. IB, immunoblotting.

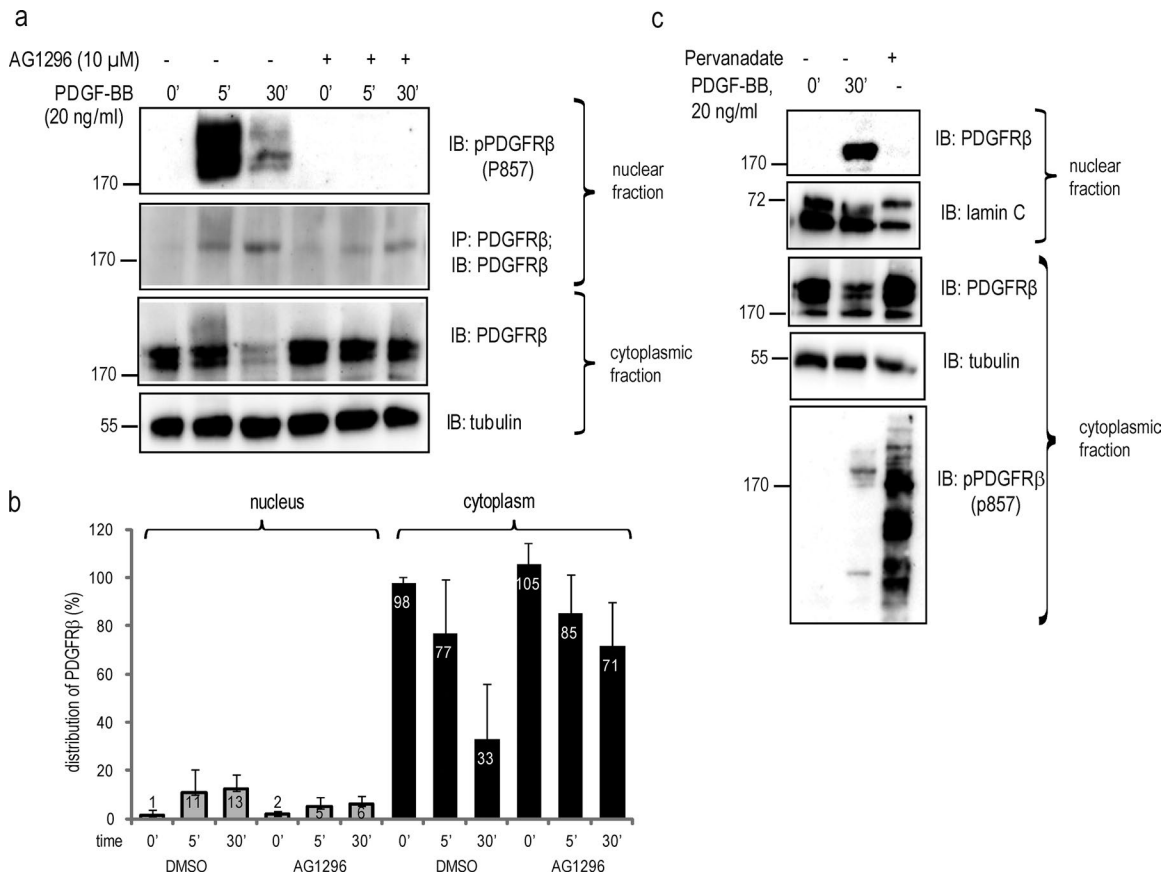


**Figure 2. PDGF-BB-induced nuclear transport of PDGFRβ is not quenched by receptor kinase inhibition.** (a) PDGFRβ translocation to the nucleus upon inhibition of PDGFRβ kinase activity. Nuclear extracts were immunoblotted for pTyr857-PDGFRβ (top) or immunoprecipitated and immunoblotted with the PDGFRβ antibody ctβ (second panel). Cytoplasmic extracts were immunoblotted for PDGFRβ with the ctβ antibody (third panel) or α-tubulin (bottom). (b) Quantification of PDGFRβ distribution upon inhibition of receptor tyrosine kinase activity with AG1296. Immunoblots were quantified as described in Fig. 1. Error bars indicate SD. Quantification was based on four independent experiments. (c) Cells were stimulated with PDGF-BB or phosphatase activity was inhibited with sodium pervanadate, and lysates were immunoblotted with total PDGFR antibody (Y92) or lamin A/C for nuclear fractions (top two panels) or total PDGFRβ, α-tubulin, and pPDGFRβ antibody for cytoplasmic fractions (three bottom panels). Molecular mass was measured in kilodaltons. IB, immunoblotting; IP, immunoprecipitation.

**PDGFRβ interacts with the Fer nonreceptor tyrosine kinase and its substrate TMF-1 in a ligand-inducible manner, affecting the composition of the SWI-SNF remodeling complex**

We could not detect any robust and reproducible binding of PDGFRβ to the promoters of known PDGF-BB-inducible genes. Instead, we found that activated PDGFRβ colocalized with the Fer kinase in the characteristic punctuate structures formed by PDGFRβ after 30 min of PDGF-BB stimulation (Fig. 6 a). We identified an interaction of PDGFRβ with Fer in both the cytoplasm and in the nucleus (Fig. 6 b), which coincided with the peak of nuclear accumulation of PDGFRβ. This suggests that nuclear PDGFRβ may transmit nuclear signals via interaction with the Fer kinase, which could further interact with chromatin (Hao et al., 1991) or chromatin-modifying proteins. Because TMF-1 was reported to be one of the substrates for Fer, we investigated interactions between PDGFRβ, Fer, and TMF-1. By coimmunoprecipitation, we demonstrated a complex between PDGFRβ and TMF-1 in the nucleus at the peak of PDGF-BB stimulation, independently of its interaction with Fer (Fig. 6 c). Immunoprecipitation (IP) of the auxiliary component of SWI-SNF complex ARID1A showed no interaction with Fer or PDGFRβ and weak interaction with

TMF-1. We also detected an interaction of PDGFRβ with TMF-1 in the cytoplasm (not depicted), which suggests that TMF-1 may be important for the cytoplasmic function of PDGFRβ as well.

TMF-1 has been reported to interact with two ATPases of the SWI-SNF remodeling complex, i.e., BRM and Brg-1 in a yeast two-hybrid system (Mori and Kato, 2002). Here, we demonstrate an interaction between TMF-1 and Brg-1 in serum-starved unstimulated fibroblasts, which was lost upon PDGF-BB stimulation (Fig. 6, d and e, IP: TMF-1), concomitant with decreased binding of Brg-1 to the core subunits of the SWI-SNF remodeling complex, BAF170 (Fig. 6 d, IP: BAF170) and BAF155 (Fig. 6 e, IP: BAF155). The interaction between Brg-1 and another subunit of the SWI-SNF remodeling complex, ARID1A (Fig. 6, d and e, IP: ARID1A), was decreased, but to a lesser extent. Thus, we suggest that by interacting with Brg-1, TMF-1 may support the transcriptionally regulatory function of the SWI-SNF complex in serum-starved cells, which becomes disassembled upon PDGF-BB stimulation, leading to activation or repression of target genes.

To investigate the importance of the kinase activity of PDGFRβ for its nuclear interactions, we performed coimmunoprecipitations between PDGFRβ, TMF-1, and Bgr-1 in the absence

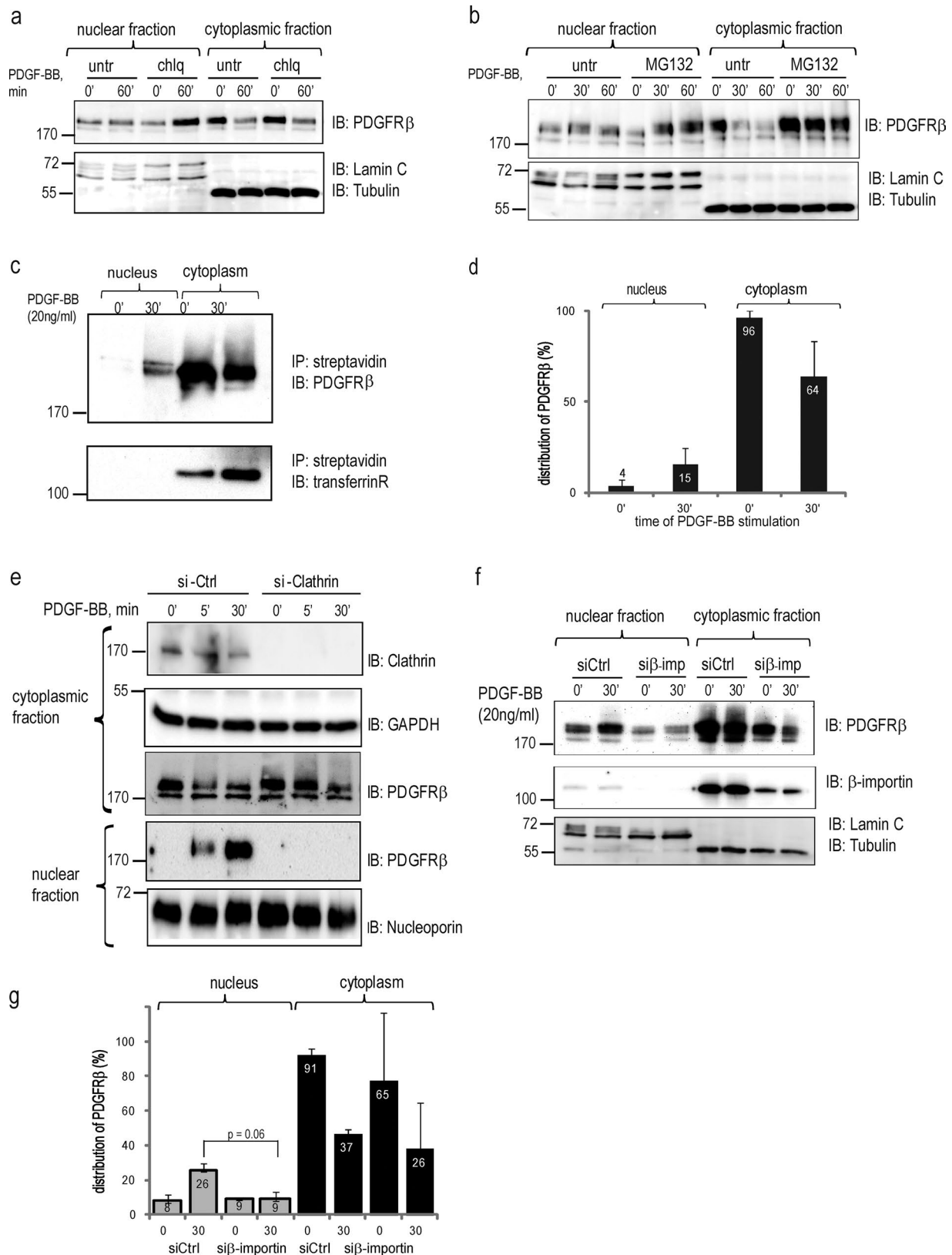


Figure 3. **Characterization of nuclear translocation pathways.** (a) PDGFRβ accumulates in the nucleus after inhibition of the endosomal-lysosomal pathway. Nuclear and cytoplasmic fractions treated or not with chloroquine (chlq) were immunoblotted with total PDGFR antibody (top), lamin A/C, and α-tubulin (bottom). A representative experiment of three biological repeats is shown. (b) Accumulation of PDGFRβ in the nucleus upon inhibition of proteasomal degradation. Nuclear and cytoplasmic fractions treated or not with MG132 were immunoblotted with total PDGFRβ antibody (top) or nuclear and cytoplasmic markers (bottom). (c) Biotinylated cell surface receptor is translocated to the nucleus. Cytoplasmic and nuclear fractions were prepared from biotinylated

or presence of AG1296. We found that the binding of PDGFR $\beta$  to TMF-1 was not inhibited by AG1296; rather, it was stabilized at 60 min of PDGF-BB stimulation (Fig. 6 f, top two blots) when PDGFR $\beta$  levels and the interaction with TMF-1 declined under normal conditions. In the same way, the complex between TMF-1 and Brg-1 was stabilized in the presence of AG1296 (Fig. 6 f). These findings suggest that the kinase activity of PDGFR $\beta$  is needed for a dynamic turnover of the repressive SWI-SNF complex over its target promoters.

### Nuclear PDGFR $\beta$ is localized in the nuclear matrix

Having found a connection between nuclear PDGFR $\beta$  and the matrix-associated SWI-SNF chromatin remodeling complex, we investigated whether PDGFR $\beta$  can itself localize to the nuclear matrix. Nuclear matrix is defined as the nuclear structure that remains after salt extraction of nuclease-treated nuclei (Reyes et al., 1997), which consists of a peripheral lamina pore complex and an internal network of filamentous ribonucleoproteins, forming a scaffold for DNA attachment (Berezney et al., 1995). When a fractionation protocol was used that allowed for separation of soluble chromatin proteins from insoluble hydrophobic nuclear matrix, we discovered that a fraction of PDGFR $\beta$  remained bound to the nuclear matrix even after the nuclear pellet was washed with 2 M NaCl (Fig. 7, top), a treatment that was used to remove all soluble proteins and unbound histones from the matrix after DNase I digestion (Fig. 7, bottom, shows a large amount of free histones in the salt wash fraction). These findings suggest that after PDGF-BB stimulation, PDGFR $\beta$  traffics from the cell surface to the nuclear matrix, where it may form a point of contact with the chromatin and interact with the transcriptional machinery and chromatin-modifying proteins.

### TMF-1-mediated chromatin remodeling leads to changes in gene transcription specific for nuclear interactions of PDGFR $\beta$

To determine the functional consequences of TMF-1-dependent rearrangement of the SWI-SNF chromatin remodeling complex, we depleted BJhTERT fibroblasts of TMF-1 with siRNA and performed RNA expression analysis of potential Brg-1 target *CDKN1A* and PDGF-BB-inducible genes based on the finding that the Brg-1-ARID1A-p53 complex serves as a key regulator of transcription of *CDKN1A* (Guan et al., 2011). We observed a transient increase in *CDKN1A* mRNA expression in response to PDGF-BB stimulation and a significant up-regulation of its transcription in cells depleted of TMF-1 (Fig. 8 a). Interestingly, up-regulation of immediate early response genes in response to PDGF-BB was not affected by the TMF-1 knockdown, as

exemplified by the known PDGF-BB-responsive genes *C-FOS* (Fig. 8 b) and *NUR77*, an orphan nuclear receptor gene with tumor-suppressing activity (Fig. 8 c; Bian et al., 2017) that we previously reported to be regulated by PDGF-BB (Eger et al., 2014). We found that although PDGF-BB stimulation suppressed the mRNA expression of *AR* in control cells, the levels of TMF-1-activated *AR* were down-regulated even more after the knockdown of TMF-1 (Fig. 8 d), as were the levels of *PDGFR $\beta$*  itself (Fig. 8 e). The efficiency of siTMF-1 mRNA knockdown is presented in Fig. 8 f. These results suggest an important novel suppressive function of TMF-1 in the regulation of expression of the cell cycle regulator *CDKN1A*, which is modulated after activation of PDGFR $\beta$ .

We further investigated the effect of canonical cytoplasmic signaling of PDGFR $\beta$  on transcription of PDGF-BB-inducible genes. After blocking Erk MAP-kinases and PI3-kinase with CI1040 and pictilisib, respectively, the transcriptional response of *C-FOS* (Fig. 8 g) was inhibited, whereas the *AR* level was unaffected (Fig. 8 h). Interestingly, the steady-state levels of *CDKN1A* were not affected, whereas its induction after 1 h of PDGF-BB stimulation was inhibited by CI1040 and pictilisib (Fig. 8 i), demonstrating that inhibition of PDGFR $\beta$  cytoplasmic signaling does not up-regulate p21, as does the knockdown of TMF-1. Thus, regulation of p21 levels during PDGFR $\beta$  activation occurs independently of cytoplasmic signaling via Erk MAP-kinase or PI3-kinase, although it is controlled by the nuclear interactors of PDGFR $\beta$ .

### Nuclear signaling of PDGFR $\beta$ promotes proliferation via a p21-dependent mechanism

To uncover a functional significance of nuclear traffic and nuclear interactions of PDGFR $\beta$ , we depleted BJhTERT fibroblasts of Fer, TMF, or Brg-1 proteins and analyzed proliferation in response to PDGF-BB (Fig. 9 a); knockdown efficiencies are presented in Fig. 9 b. We found that the proliferative response of cells was severely inhibited by the knockdown of each of the interacting proteins. We also investigated a possible functional mechanism of inhibition of proliferation and found an increased number of cells expressing p21 protein after knockdown of Fer (21%; Fig. 9 d), TMF-1 (25%; Fig. 9 e), or Brg-1 (50%; Fig. 9 f) as compared with the control cells (6.5%; Fig. 9 c); quantification is presented in Fig. 9 g. These findings demonstrate the importance of the Fer-TMF-1-Brg-1 axis for the regulation of p21 levels and proper progression of the cell cycle and establishes a function of PDGFR $\beta$  in the regulation of the cell cycle by its nuclear interactions with Fer and TMF-1.

cells stimulated with PDGF-BB. Biotinylated proteins were precipitated with streptavidin agarose and immunoblotted for total PDGFR $\beta$  (top) or transferrin receptor (bottom). (d) Quantification of the distribution of biotinylated PDGFR $\beta$  was performed as described in Fig. 1 b. Error bars indicate SD. (e) Nuclear translocation of PDGFR $\beta$  is inhibited by siRNA knockdown of clathrin. The efficiency of clathrin siRNA knockdown was determined with an anticlathrin antibody (top). The levels of PDGFR $\beta$  in the cytoplasmic and nuclear fractions were determined by immunoblotting (middle). The purity of the fractions was confirmed by immunoblotting for GAPDH (a cytoplasmic marker) or lamin A/C. (f) Nuclear translocation of PDGFR $\beta$  is decreased upon siRNA knockdown of  $\beta$ -importin. The level of PDGFR $\beta$  in the cytoplasmic and nuclear fractions was determined by immunoblotting with total PDGFR antibody (top); the purity of fractionations was confirmed by blotting for lamin A/C and  $\alpha$ -tubulin (bottom). The efficiency of the knockdown was determined by immunoblotting with anti- $\beta$ -importin antibody (middle). (g) Quantification of PDGFR $\beta$  distribution upon  $\beta$ -importin siRNA knockdown was performed as described above and was based on three independent experiments. Molecular mass was measured in kilodaltons. Error bars indicate SD. IB, immunoblotting; IP, immunoprecipitation.



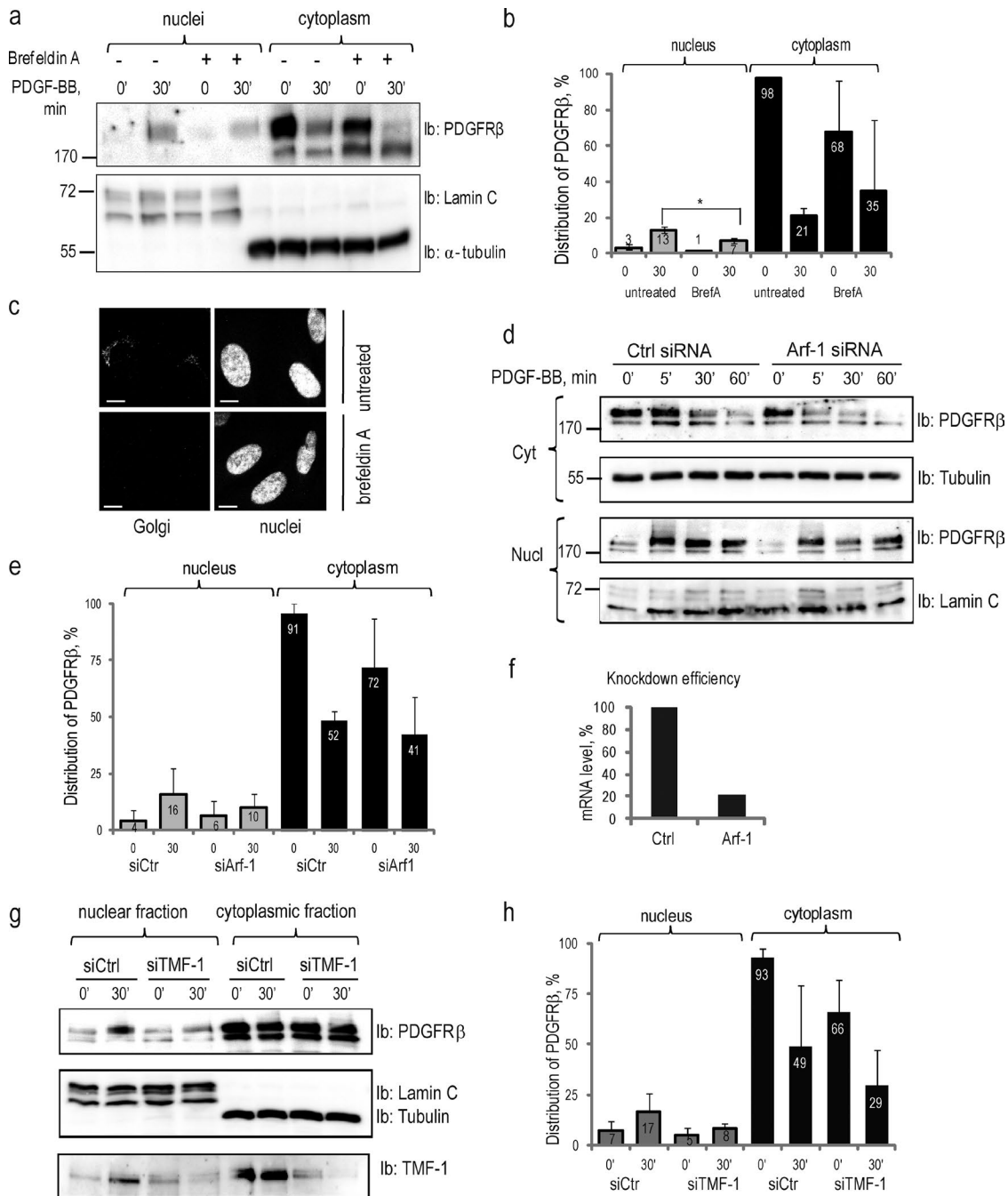


Figure 4. **Nuclear translocation of PDGFRβ is dependent on intact Golgi and retrograde transport system.** (a) Inhibition of nuclear translocation of PDGFRβ upon brefeldin A treatment. Nuclear and cytoplasmic fractions of cells treated or not with brefeldin A were immunoblotted for PDGFRβ (top) and markers (bottom). (b) Quantification of the distribution of PDGFR in the nucleus and the cytoplasm upon treatment with brefeldin A was performed, as described above, for three independent experiments. \*,  $P < 0.05$ , two-tailed  $t$  test. (c) The integrity of the Golgi apparatus was lost upon treatment with brefeldin A. Golgi (top left) was absent after the treatment with brefeldin A (bottom left); nuclei are presented on images to the right. Bars, 10  $\mu$ m. (d) PDGFRβ translocation to the nucleus is decreased upon siRNA knockdown of Arf-1. Cytoplasmic (two top panels) and nuclear (two bottom panels) fractions were immunoblotted for PDGFRβ; the purity of the fractions was determined by immunoblotting for  $\alpha$ -tubulin and lamin C. (e) Nuclear distribution of PDGFRβ upon Arf-1 knockdown was quantified based on three independent experiments. (f) The efficiency of Arf-1 depletion was confirmed by quantitative PCR. The mean mRNA level in knockdown samples was calculated as a percentage relative to the mean mRNA levels in control samples. (g) Nuclear translocation of PDGFRβ is decreased upon siRNA knockdown of TMF-1. Nuclear and cytoplasmic fractions were immunoblotted with PDGFRβ antibody (top) or lamin A/C and  $\alpha$ -tubulin (middle). The efficiency of TMF-1 knockdown was demonstrated by immunoblotting with TMF-1 antibody (bottom). (h) The distribution of PDGFRβ in the nucleus and cytoplasm upon depletion of TMF-1 was quantified as described above based on three independent experiments. Molecular mass was measured in kilodaltons. Error bars indicate SD. Ib, immunoblotting.



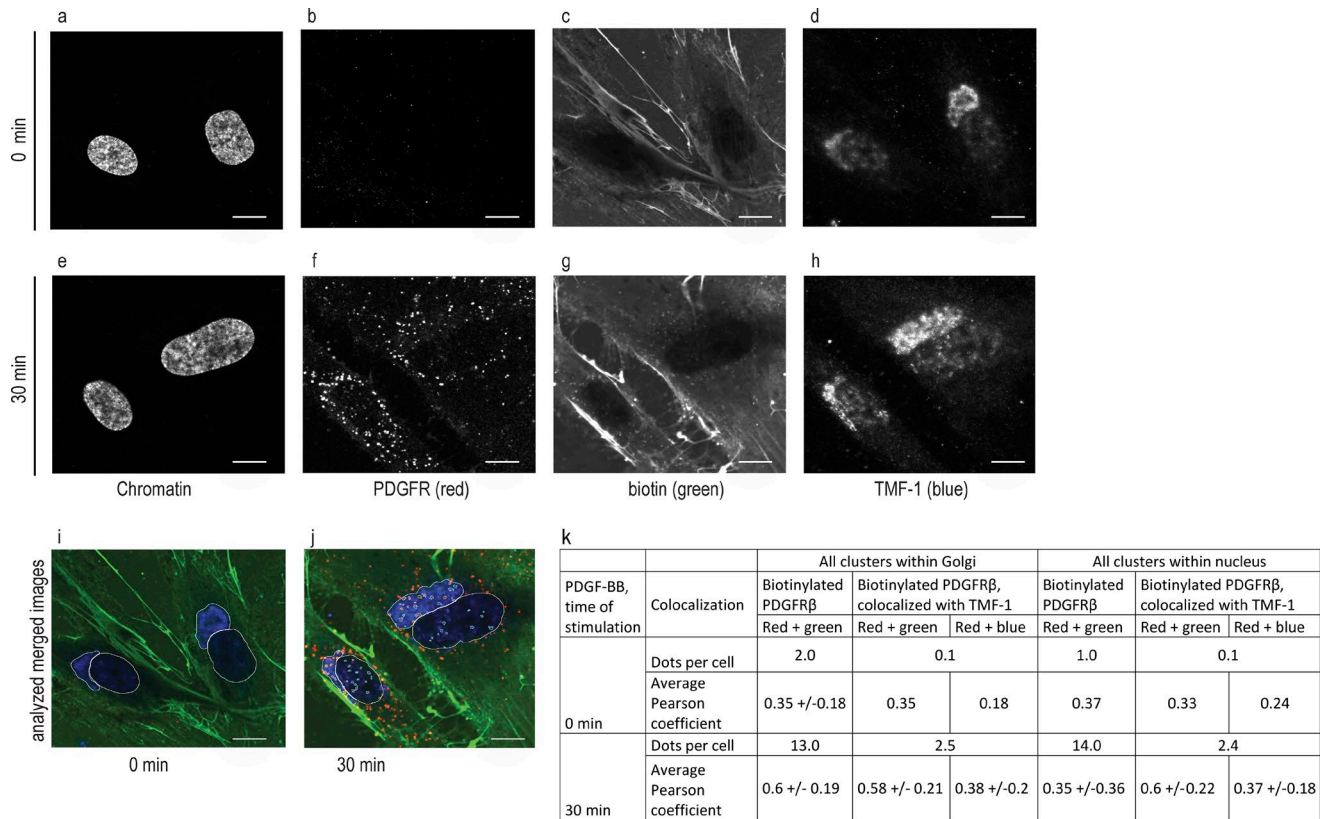


Figure 5. **Biotinylated PDGFR traffics to the nucleus via TMF-1-positive Golgi vesicles.** Biotinylated cells were stimulated (e–h) or not (a–d) with PDGF-BB and immunostained for biotin, PDGFR $\beta$ , TMF-1, and DAPI. Original black and white images (a–h) were uploaded into an automatic pipeline at Cell Profiler for quantification of colocalization. The merged image that was created by the software is presented, where Golgi area (as detected by TMF-1) and nucleus (as detected by DAPI) were isolated and PDGFR $\beta$  clusters were analyzed within these areas for unstimulated (i) and stimulated (j) cells. The mean number of dots and mean Pearson correlation coefficients for these dots (pairwise for red, green, and blue channels) were calculated and presented in the table (k). Bars, 10  $\mu$ m.

## Discussion

In addition to the well-characterized signaling from the plasma membrane and endosomes by RTKs, ligand-induced nuclear localization has been described for several of the members (Carpenter and Liao, 2013). Full-length receptors found in the nucleus include EGFR, ErbB2, ErbB3, FGF receptors (FGFR1, FGFR2), IGF-1R, Met, and VEGF receptors (VEGFR1 and VEGFR2; Carpenter and Liao, 2013). In this study, we showed that in response to PDGF-BB stimulation, the full-length PDGFR $\beta$  translocates to the nucleus. Nuclear translocation was not absolutely dependent on the receptor kinase activity of PDGFR $\beta$ , and PDGFR $\beta$  phosphorylation, promoted by phosphatase inhibition in the absence of ligand binding, did not lead to nuclear translocation. Together, these observations suggest that dimerization of receptors is essential for nuclear translocation, whereas receptor kinase activity is not; however, the kinase activity has a functional role in the nucleus. Our data suggest that the nuclear receptor is derived from the cell surface and is dependent on clathrin coating of vesicles and TMF-1 tethering. Similarly, EGFR (De Angelis Campos et al., 2011) and IGF-1R (Aleksic et al., 2010) translocate to the nucleus in clathrin-dependent manners. Clathrin plays an essential role in budding off vesicles within the intra-Golgi network, whereas TMF-1 acts by capturing and tethering cargo vesicles, connecting them to their destination organelles. In relocation studies, TMF-1 demonstrated specificity for Golgi resident proteins and for some of the endosomes-to-Golgi

cargo (Wong and Munro, 2014). TMF-1 also plays a critical role in the Rab6-dependent retrograde transport of Shiga toxin from early recycling endosomes to the trans-Golgi network and from Golgi to the ER (Yamane et al., 2007; Miller et al., 2013). Thus, it seems feasible that internalized PDGFR $\beta$  is directed to the nucleus via TMF-1-positive Golgi vesicles, representing the retrograde transport machinery.

Additionally, we observed a decrease in nuclear translocation of PDGFR $\beta$  after efficient knockdown of  $\beta$ -importin, which is one of the major mediators of protein nuclear transport via the nuclear pore complex (Kimura and Imamoto, 2014). A role of  $\beta$ -importin in the nuclear translocation was also shown for EGFR (Lo et al., 2006), ErbB-2 (Giri et al., 2005), c-Met (Gomes et al., 2008), IGF-1R (Packham et al., 2015), and FGFR-1 (Stachowiak et al., 2007), suggesting that  $\beta$ -importin plays a general role in the translocation of cell surface RTKs to the nucleus. As was suggested for EGFR,  $\beta$ -importin may interact with retrograde-transported vesicles and facilitate their traffic toward the nucleus (Wang et al., 2010c); thus, there may be no direct interaction of  $\beta$ -importin with PDGFR $\beta$  of the kind that occurs for soluble proteins.

Despite the accumulating data about nuclear traffic of transmembrane receptors, it has been difficult to explain the presence and the function of hydrophobic receptors in the soluble nucleoplasm. Our findings offer a possible explanation for the nuclear presence and function of transmembrane receptors. The nuclear

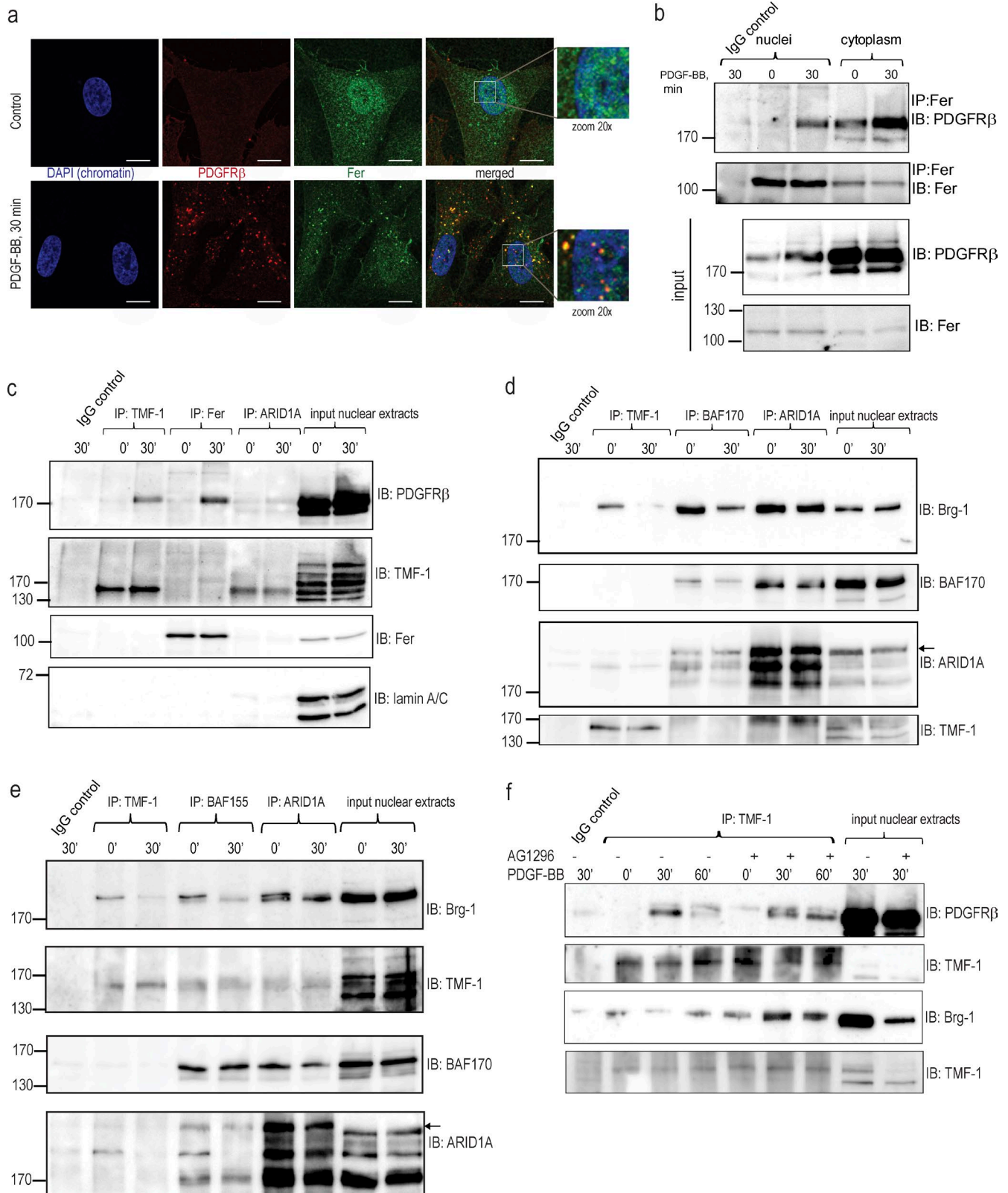


**Figure 6. PDGFR $\beta$  forms ligand-dependent complex with Fer and TMF-1, affecting composition of the SWI-SNF remodeling complex. (a)** Immunofluorescence staining of colocalization of PDGFR $\beta$  and Fer kinase. PDGFR $\beta$  was immunostained with extra PDGFR $\beta$  (red), chromatin with DAPI (blue), and the Fer kinase was stained in green. Yellow indicates colocalization between PDGFR $\beta$  and Fer. Bars, 10  $\mu$ m. **(b)** Coimmunoprecipitation of PDGFR $\beta$  and Fer kinase in the nucleus and in the cytoplasm. Immunoprecipitated complexes were immunoblotted for PDGFR $\beta$  (top) or Fer (second panel). 10% of the input material was analyzed by immunoblotting for PDGFR $\beta$  and Fer (two bottom panels). **(c)** PDGFR $\beta$  forms PDGF-BB-inducible complexes with TMF-1 and Fer in the nucleus.

matrix serves as the internal scaffold of the nucleus, anchoring the origin of replication sites, core enhancers, transcription factors, and matrix- and scaffold-associated DNA regions that function as control elements for transcriptional domains (Laemmli et al., 1992; Forrester et al., 1994; Boulikas, 1995). In addition, full-length FGFR1 and several unidentified proteins with tyrosine kinase activity have been localized to the nuclear matrix (Stachowiak et al., 1996a,b), including nonreceptor tyrosine kinases of the Src family (Radha et al., 1996; Nakayama et al., 2006). It was also shown that ATP-dependent release of the SWI-SNF complex from its nuclear targets is a result of a cascade of kinase activities, and hyperphosphorylation of Brg-1 and BRM leads to their release from the tight association with the nuclear matrix that coincides with the start of mitosis (Reyes et al., 1997). The nuclear matrix may thus serve as a docking site for PDGFR $\beta$  in the nucleus, whereas the intracellular part of the receptor may freely interact with either its binding partners or phosphorylation targets, or directly with the chromatin. Interestingly, in our fractionation experiments, a certain amount of PDGFR $\beta$  was detected not only at the nuclear matrix but also in the chromatin fraction, suggesting that PDGFR $\beta$  could also maintain direct interactions with the chromatin.

In this work, we have uncovered an inducible nuclear protein complex of PDGFR $\beta$  with both nonreceptor tyrosine kinase Fer and its substrate TMF-1, suggesting that the effect of PDGFR $\beta$  on chromatin may be partially mediated through these interactions. Fer caused tyrosine phosphorylation of TMF-1, with no direct interaction between endogenous Fer and TMF-1 being detected (Schwartz et al., 1998), consistent with our observations. Thus, the interaction between Fer and TMF-1 could be transient, or phosphorylation of TMF-1 by Fer could be mediated by PDGFR $\beta$ .

We have demonstrated that the formation of a PDGFR $\beta$ -TMF-1 complex correlates with changes in the composition of the SWI-SNF remodeling complex, which loses its binding to TMF-1 concomitant with the release of Brg-1 after PDGF-BB stimulation. The transient character of this interaction is dependent on the kinase activity of PDGFR $\beta$  because its inhibition led to stabilization of PDGFR $\beta$  binding to TMF-1 and TMF-1 to the SWI-SNF chromatin remodeling complex. The SWI-SNF complex is extensively regulated by different signaling pathways (Simone, 2006) and can repress or activate multiple genes depending on which transcription factors and modulators it recruits. A possible mechanism behind the changes in SWI-SNF composition could be that phosphorylation of TMF-1 by Fer and/or PDGFR $\beta$  promotes disruption of the TMF-1-containing repressive SWI-SNF complex; this may lead to release of Brg-1 followed by its binding to p53, which activates the transcription of *CDKN1A*, although interaction with

the kinase inactive receptor may maintain a repressive SWI-SNF complex and inhibit p21 expression. Transient up-regulation of p21 in response to PDGF-BB may represent a feedback mechanism regulating proper cell cycle progression, which also has been observed in NIH 3T3 (Yu et al., 2003). We speculate that when Fer, TMF-1, or Brg-1 was depleted, the inhibitory SWI-SNF protein complex on the p21 promoter could not be maintained, which led to up-regulation of mRNA transcription even in unstimulated cells. Of note, we observed that the knockdown of Fer, TMF-1, or Brg-1 significantly decreased proliferation of fibroblasts in response to PDGF-BB, which was explained by up-regulation of the number of cells expressing p21 that may cause cell cycle block. TMF-1 has been reported to act as a tumor suppressor in cancer models (Abrham et al., 2009) and to suppress proliferation (Perry et al., 2004; Volpe et al., 2006), although we found a growth-suppressing effect in the absence of TMF-1, which demonstrates the complexity of pro- and antiproliferation signaling involving TMF-1-mediated growth control. Our results suggest a novel function of the Fer-TMF-1-Brg-1 axis in the regulation of tumor suppressor p21, which controls the progression of the cell cycle and is transiently regulated by the nuclear presence of PDGFR $\beta$ .

Interestingly, PDGF-BB-induced up-regulation of immediate early gene expression was not affected by the knockdown of TMF-1, as it was by inhibition of cytoplasmic PDGFR $\beta$  signaling via Erk MAP-kinase and PI3-kinase. It was postulated that the large group of immediate early genes is constitutively poised for transcription and does not require SWI-SNF-dependent chromatin remodeling to be transcribed (Ramirez-Carrozzi et al., 2009; Fowler et al., 2011). Thus, nuclear translocation of PDGFR $\beta$  and its interaction with TMF-1 implies that transcription of cell cycle regulators and subsequent progression of the cell cycle is not solely dependent on activation of cytoplasmic signaling pathways. In conclusion, we show that PDGFR $\beta$  traffics to the nucleus after PDGF-BB treatment. The presence of PDGFR $\beta$  in the nucleus may catalyze specific regulatory events at the nuclear matrix and chromatin that are necessary for modulation of gene transcription in response to growth stimuli. These findings have implications for our understanding of the mechanisms whereby PDGFRs regulate cell growth and proliferation.

## Materials and methods

### Cell culture, drug treatments, and PDGF stimulation

Normal human foreskin fibroblasts BJhTERT (Clontech) were used in all experiments except Fig. S3. Cells were cultured in DMEM (GIBCO BRL) supplemented with 10% FBS, 100 U/ml

TMF-1, Fer, and ARID1A immunocomplexes were immunoblotted for PDGFR $\beta$ , TMF-1, and Fer. 10% of the input lysate was loaded on the last two lanes on each blot; nuclear TMF-1 was poorly detected by direct immunoblotting as opposite to immunoblotting after IP. The membrane was reblotted for lamin A/C as a loading control. **(d)** Dissociation of TMF-1-Brg-1 and Brg-1-BAF170 nuclear complexes upon PDGF-BB stimulation. TMF-1, BAF170 and ARID1A immunocomplexes were immunoblotted for Brg-1 and reblotted for BAF170 or blotted for ARID1A and reblotted for TMF-1. 10% of the input lysate was loaded on each gel. Arrows indicate ARID1A protein. **(e)** Dissociation of TMF-1-Brg-1 and Brg-1-BAF155 nuclear complexes upon PDGF-BB stimulation. This experiment reproduces the result from d, but an antibody against the BAF155 core subunit of SWI-SNF chromatin remodeling complex was used instead of BAF170 for IP. Arrows indicate ARID1A protein. **(f)** Kinase-inactive PDGFR $\beta$  binds TMF-1 and prevents PDGF-BB-inducible dissociation of the SWI-SNF complex. Cells were pretreated with AG1296 and stimulated with PDGF-BB. TMF-1 immunocomplexes from nuclear extracts were blotted for PDGFR $\beta$  (top) and reblotted for TMF-1 (second) or blotted for Brg-1 (third) and reblotted for TMF-1 (bottom). Molecular mass was measured in kilodaltons. IB, immunoblotting; IP, immunoprecipitation.



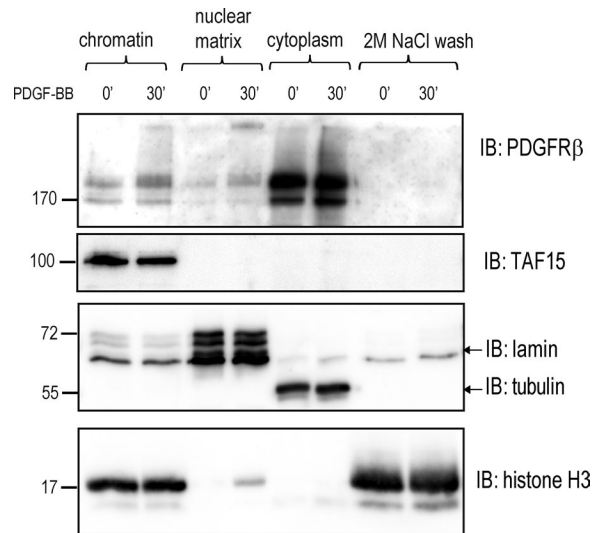


**Figure 7. PDGFR $\beta$  in the nucleus is localized to the chromatin and nuclear matrix.** Chromatin, nuclear matrix, cytoplasmic fractions, and 2 M NaCl wash eluate were immunoblotted for PDGFR $\beta$ . RNase II cofactor TATA-associated factor 15 (TAF15), lamin A/C,  $\alpha$ -tubulin, and histone H3 were used as markers for transcriptionally active chromatin, nuclear matrix, cytoplasm, and soluble chromatin, respectively. Molecular mass was measured in kilodaltons. IB, immunoblotting.

penicillin, and 100  $\mu$ g/ml streptomycin and were routinely tested for mycoplasma contamination and found negative. Cells were seeded in 100-mm Petri dishes, starved in DMEM, supplemented with 0.1% FBS overnight, and stimulated at 50% confluence with 20 ng/ml of recombinant human PDGF-BB (gift from Amgen) for the indicated periods of time. To interfere with activation of PDGFR $\beta$ , cells were pretreated with the specific PDGFR $\beta$  kinase inhibitor AG1296 (10  $\mu$ M) for 1 h before PDGF-BB stimulation. To enhance receptor phosphorylation in the absence of PDGF-BB stimulation, cells were treated with sodium pervanadate (1 mM hydrogen peroxide and 0.1 mM vanadate, freshly mixed) for 30 min. To block Golgi to ER retrograde traffic, cells were pretreated with 500 ng/ml brefeldin A (Sigma) for 1.5 h before PDGF-BB stimulation. To block lysosomal or proteasomal degradation, cells were pretreated for 3 h with 100  $\mu$ M chloroquine or 25  $\mu$ M MG132, respectively. To inhibit cytoplasmic signaling of PDGFR $\beta$ , cells were pretreated with 3  $\mu$ M Erk1/2 MAP-kinase inhibitor CI1040 (Selleckchem) or 2  $\mu$ M PI3-kinase inhibitor pictilisib (Selleckchem) before stimulation with PDGF-BB.

#### Antibodies

The following antibodies were used for the detection of total PDGFR $\beta$ : homemade rabbit polyclonal antibody, raised against a GST fusion of the C-terminal part of PDGFR $\beta$  (denoted ct $\beta$ ; 78) and purified on a protein A agarose column (Pierce; used for IP and immunoblotting of streptavidin pull-downs); rabbit monoclonal anti-PDGFR $\beta$  clone Y92 (ab32570, Abcam; raised against the intracellular part of the PDGFR $\beta$ -abbreviated intra-PDGFR $\beta$  antibody, used for all immunoblots and immunofluorescence in Figs. 1 d and S1); polyclonal rabbit anti-PDGFR $\beta$  (sc-339; Santa Cruz, discontinued; used for immunofluorescence in Fig. 1 e); goat anti-PDGFR $\beta$  (AF358; R&D; raised against the extracellular

part of PDGFR $\beta$ -abbreviated extra-PDGFR $\beta$  antibody, used for immunofluorescence in Figs. 1 d, 5 a, 9, and S2 c); mouse anti-PDGFR $\beta$  antibody (MAB1262; R&D; used for immunofluorescence in Fig. 5); and antiphospho-PDGFR $\beta$  site pTyr857 (Cell Signaling; used for immunoblotting). PDGFR $\beta$  detection in the nucleus was consistently reproduced by all antibodies used. Phosphotyrosine-specific mouse monoclonal antibody PY99, mouse anticlathrin heavy chain, mouse antikaryopherin (Kpn or  $\beta$ -importin), p21, and rabbit Fer antibody were from Santa Cruz. Antibodies against lamin A/C, Histone H3, Brg-1, BAF170, BAF155, and ARID1A were purchased from Cell Signaling, antibodies against TMF-1 were from ProteinTech,  $\alpha$ -tubulin was from Sigma, and the anti-mouse organelle detection kit was from BD Transduction. Fluorescent antibodies were streptavidin-Alexa Fluor 488, anti-mouse IgG-Alexa Fluor 488 (green), anti-rabbit IgG-Alexa Fluor 546 (red), anti-rabbit Alexa Fluor 594 (red), and anti-rabbit Alexa Fluor 633 (far red) from ThermoScientific.

#### siRNA knockdown

For the knockdown of clathrin, cells were seeded in 100-mm Petri dishes and transfected the next day at ~50% confluence with 20 nM clathrin heavy chain Silencer Select siRNA (Invitrogen) using 5  $\mu$ l of SilentFect reagent (BioRad) in 10% FBS in DMEM. The next day, the media were replaced with 0.1% FBS in DMEM, and on day 2, cells were replated and retransfected with 20 nM siRNA, serum starved for 3 d, stimulated with PDGF-BB, and collected for nuclear fractionation. As control knockdown, stealth RNAi negative control #12935112 (Invitrogen) was used. For the knockdown of  $\beta$ -importin, cells were seeded as above and transfected with a mix of three siRNAs (4 nM each) from the Tri-silencer siRNA kit (Origene) using 5  $\mu$ l of SilentFect reagent; the negative control was used as provided in the kit. The medium was replaced with 0.1% FBS in DMEM, and cells were stimulated with PDGF at 6 d after knockdown and collected for nuclear fractionation. For the knockdown of Arf-1, Fer, TMF-1, and Brg-1, cells were transfected with Tri-silencer siRNA kits in the same ways as for Kpn, but analyzed at 3 d after knockdown. Levels of the knockdown were analyzed by immunoblotting (clathrin, Fer, TMF-1, Brg-1, and  $\beta$ -importin) or quantitative PCR (Arf-1 and TMF-1).

#### Subcellular fractionation

Cells were seeded, starved, and stimulated as described above, washed two times with cold PBS, lysed in 1 ml of cytoplasmic lysis buffer (10 mM MES, pH 6.2, 10 mM NaCl, 1.5 mM MgCl<sub>2</sub>, 1 mM EDTA, 5 mM DTT, 1% Triton X-100, 1 mM pefablock [Sigma], and 1 mM NaF) for 10 min on ice, scraped into Eppendorf tubes, and centrifuged for 10 min at 3,000 rpm in a bench-top centrifuge. The supernatant was recentrifuged at 13,000 rpm for 20 min and collected as the cytoplasmic fraction. The pellet from the first centrifugation (nuclei) was washed three times with 1 ml of cytoplasmic lysis buffer supplemented with 1% NP-40 and once with cytoplasmic lysis buffer without addition of detergents. The purified nuclear pellet was resuspended in 0.5 ml of nuclear extraction buffer (25 mM Tris-HCl, pH 10.5, 1 mM EDTA, 0.5 M NaCl, 5 mM  $\beta$ -mercaptoethanol, and 0.5% Triton X-100), vortexed for 10 min at 4°C, and centrifuged for 20 min at 13,000 rpm, and the supernatant was collected as a nuclear fraction.



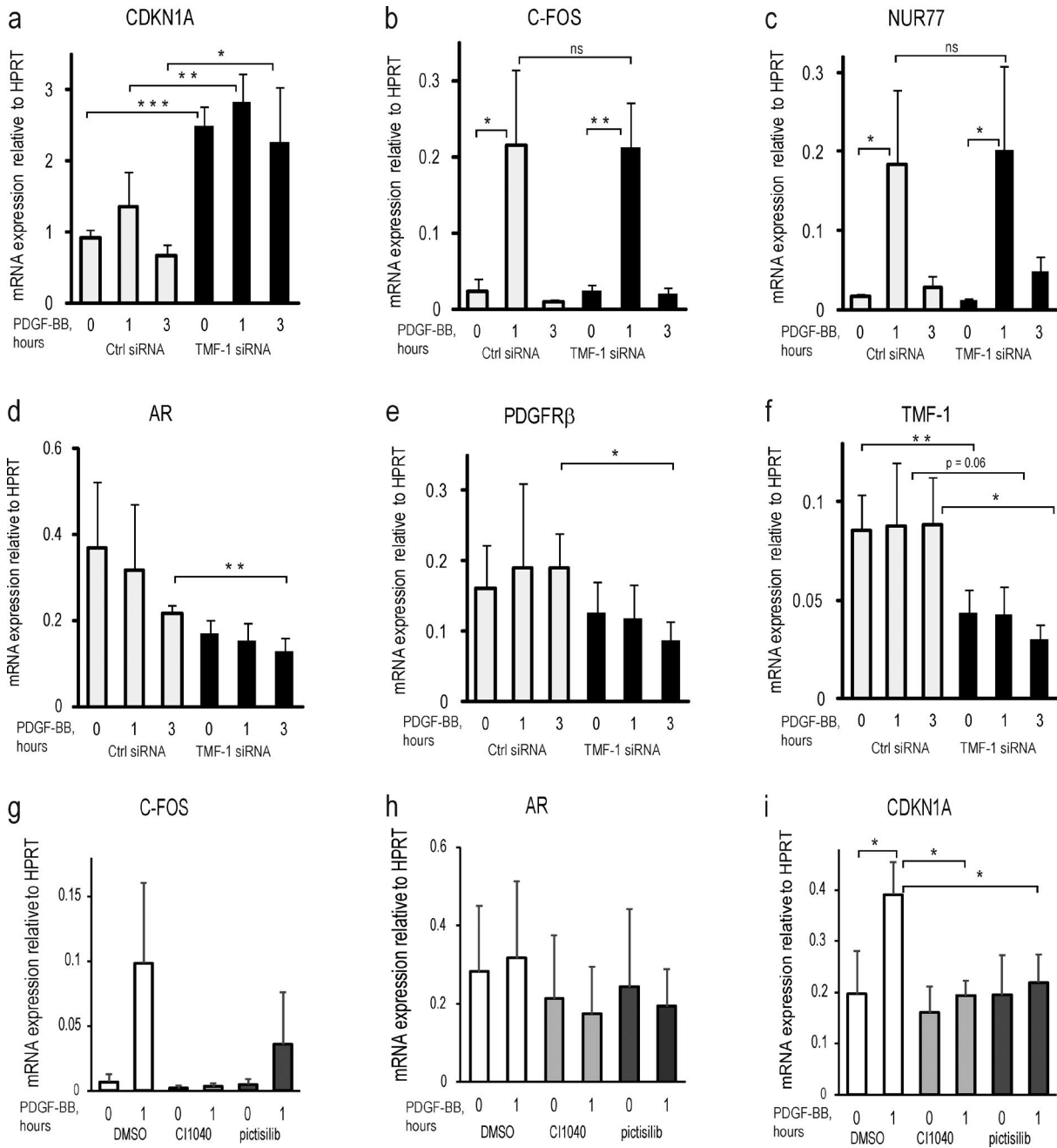


Figure 8. **Transcriptional analysis of target genes during PDGF-BB stimulation at TMF-1 knockdown or inhibition of PDGFR $\beta$  kinase activity and cytoplasmic signaling via Erk1/2 and PI3-kinase.** Cells were transfected with control (white bars) or TMF-1 (black bars) siRNA (a–f) or pretreated with C1040 (light gray bars) and pictilisib inhibitor (dark gray bars; g–i) before stimulation with PDGF-BB. mRNA expression of the following genes was analyzed by quantitative PCR to test for the knockdown efficiency: *CDKN1A*, *C-FOS*, nuclear receptor *NUR77*, *AR*, *PDGFR $\beta$* , and *TMF-1*.  $\Delta\Delta Ct$  was calculated as a  $\log_2$  of the difference between cycle threshold values of a reference gene HPRT and a gene of interest. The levels of expression represent an average signal obtained from four biological replicates with SD indicated on the graph. Two-tailed *t* test statistical analysis was performed for the difference between mRNA expression levels of *CDKN1A* in control cells versus siTMF knockdown cells. \*,  $P < 0.05$ ; \*\*,  $P < 0.01$ ; \*\*\*,  $P < 0.001$ . ns, not significant.

This protocol was specifically optimized and regularly tested for the nuclear fraction not to contain any contamination of Golgi, ER, lipid rafts, and other organelles.

#### Immunoblotting

Equal volumes of cytoplasmic and nuclear extracts (adjusted by blotting with cytoplasmic and nuclear markers) were boiled in SDS sample buffer containing 10 mM DTT and separated by

SDS-PAGE. Proteins were electrotransferred to polyvinylidene difluoride membrane (Immobilon P) and blocked for 1 h in 5% BSA in PBS containing 0.04% Tween 20. Membranes were incubated with primary antibody, diluted in 1% BSA in PBS at 4°C overnight, washed three times in PBS, and incubated with horseradish peroxidase-conjugated anti-rabbit (1:40,000 dilution) or anti-mouse (1:25,000 dilution) antibody (Amersham Pharmacia). Proteins were visualized using Super Signal West

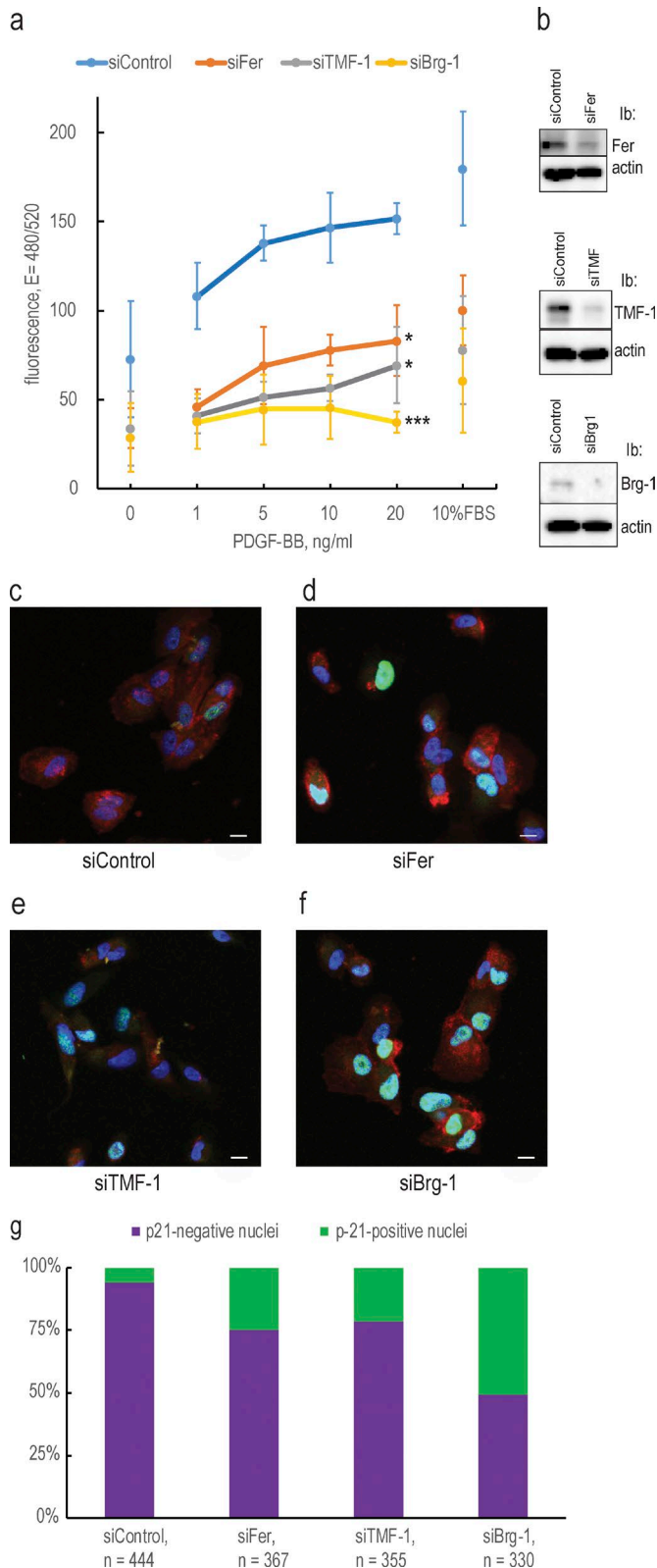


**Figure 9. The Fer-TMF-1-Brg-1 axis regulates proliferation by controlling p21 protein levels.** (a) Knockdown of Fer, TMF-1, and Brg-1 inhibit proliferation in response to PDGF-BB and serum. Proliferative response was evaluated by measuring incorporation of a fluorescent DNA-binding dye; fluorescence values were plotted against increasing concentrations of PDGF-BB. The statistical significance of the difference between control and knockdown

Dura ECL substrate (ThermoScientific), and membranes were scanned with a charge-coupled device camera Intelligent Dark Box II (Fujifilm). Raw data files were exported as TIFF files from Aida software, and level autocontrast was applied to the blots using Photoshop (Adobe).

**IP and coimmunoprecipitation**

Nuclear extracts were prepared as described in the subcellular fractionation protocol with the following modifications. Cytoplasmic buffer was 10 mM MES, pH 6.2, 10 mM NaCl, 1.5 mM MgCl<sub>2</sub>, 1 mM EDTA, 1% Triton X-100, and 1× Halt protease inhibitor cocktail (ThermoScientific); washing buffer was the same as cytoplasmic but without detergents; and nuclear extraction buffer was 25 mM Tris-HCl, pH 7.5, 1 mM EDTA, 0.5 M NaCl, 0.5% Triton X-100, and 1× Halt protease inhibitor cocktail. Nuclear extracts were diluted two times with neutralization buffer (100 mM Tris-HCl, pH 7.4, and 0.5% Triton X-100), and equal volumes of cytoplasmic (where applicable) or nuclear fractions were incubated overnight at 4°C with the antibodies at 1:100 dilution. 50 µl of 50% protein G-Sepharose slurry was added, and incubation was prolonged for 1 h at 4°C; beads were washed three times in IP washing buffer (10 mM Tris-HCl, pH 7.4, 250 mM NaCl, and 0.5% Triton X-100) and eluted in 40 µl of sample buffer containing 10 mM DTT. Eluates were resolved by SDS-PAGE and subjected to immunoblotting as described above.

**Biotinylation of cell surface PDGFRβ**

Cells were seeded in Petri dishes as above and starved overnight in DMEM supplemented with 0.1% FBS and washed two times in cold PBS. Cell-surface proteins were then biotinylated by incubation with 0.2 µg/ml EZ-link Sulfo-SS-Biotin (ThermoScientific). After 1 h at 4°C, biotinylation was blocked with 50 mM Tris-HCl, pH 7.5, warm media was replaced, and cells were stimulated with PDGF-BB for the indicated time periods. Cells were lysed and processed for nuclear fractionation. For analysis by immunofluorescence (Fig. 5), remaining cell surface biotin was stripped with 100 mM sodium 2-mercaptoethanesulfonate (MESNA) in 10 mM Tris, pH 7.0, 100 mM NaCl, and 1 mM EDTA at RT for 5 min; slides were fixed and processed as described below.

**Immunofluorescence**

Cells were grown on 10 × 10-mm coverslips, starved, and stimulated with 20 ng/ml PDGF-BB. Cells were then fixed in 3.5% paraformaldehyde for 10 min at RT, washed two times in PBS, and immunostained. For that, coverslips were permeabilized in 1 ml PBS, supplemented with 1% BSA and 0.1% SDS for 15 min at RT, and then blocked in 1 ml PBS supplemented with 1% BSA at

cells at 20 ng/ml PDGF-BB was analyzed with two-tailed *t* test. Error bars indicate SD. \*, *P* < 0.05; \*\*\*, *P* < 0.001. (b) The efficiencies of the knockdowns were determined by immunoblotting. lb, immunoblotting. (c-f) Immunostaining of p21 protein expression upon Fer, TMF-1, and Brg-1 knockdown. Cells treated with control siRNA or siRNA for Fer, TMF-1, or Brg-1 were stained for p21 protein (green) and PDGFRβ (red); chromatin was stained with DAPI (blue). Bars, 10 µm. (g) The percentage of p21-expressing cells was counted using the automatic pipeline in Cell Profiler.

RT for 45 min. Primary antibody at a 1:100 dilution was applied in PBS supplemented with 1% BSA overnight at 4°C. Coverslips were washed five times in PBS and incubated with a 1:200 dilution of fluorescent secondary antibody in 1% BSA in PBS for 50 min. Coverslips were washed five times with PBS, mounted with one drop of Vectashield mounting media with DAPI (Vector Labs), and analyzed by confocal microscopy.

### Microscope image acquisition and processing

Images were acquired using ZEISS LSM510 (Figs. 1 g and S1) and LSM700 (Figs. 1 d, 4 c, 5 a–j, 6 a, 9 c–f, and S2 c) inverted confocal microscopes with numerical aperture 1.4 oil objectives at the Biological Visualization Facility at 512 × 512 and 1,128 × 1,128 pixels, respectively, at RT using Zen black software and a high-resolution AxioCam microscope camera (ZEISS). Images were exported as merged TIFF files with 8-bit resolution. Images were separated according to their colors in Photoshop software, and adjustment of brightness of individual color channels was performed equally on all images within each experiment.

For quantification of colocalization (Fig. 5), original black and white individual channel images were uploaded into Cell Profiler imaging software (Carpenter et al., 2006), and an automatic pipeline was created at the SciLife BioImage Informatics Facility, whereby TMF-1 staining was used to isolate regions of Golgi and DAPI staining was used to isolate the nucleus. Dot-like clusters of PDGFR $\beta$  were circled by the pipeline, and pairwise correlation was analyzed for PDGFR-biotin and PDGFR-TMF-1 channels within the circled areas. Correlation was evaluated by calculating the Pearson correlation coefficient, which is >0 for the possibility of colocalization and equal to 1 when the correlation is perfect. To increase the credibility of identified triple colocalized dots, the cutoff for triple colocalizations was placed at 0.2, meaning that the Pearson coefficient for each pair of channels for a triple colocalized dot was >0.2. The images presented in the figure were merged into an RGB image by the software.

For counting p21-expressing cells (Fig. 9), an automatic pipeline for Cell Profiler was created with the help of the SciLife BioImage Informatics Facility, whereby all DAPI-positive nuclei were counted versus p21-expressing nuclei (Fig. 9, c–g, colored in green) on RGB confocal fluorescent images, taken as described above.

### Nuclear matrix isolation

Isolation of chromatin and nuclear matrix fractions was performed according to Reyes et al. (1997) with some modifications. Cells were grown in 100-mm Petri dishes, starved overnight at 50% of confluence, and stimulated with 20 ng/ml PDGF-BB for 30 min. After two washes in PBS, cells were extracted in 1 ml cytoplasmic extraction buffer (as described in the subcellular fractionation protocol) and washed once with the same buffer without detergents. The pellet was resuspended in 200  $\mu$ l cytoplasmic lysis buffer (10 mM MES, pH 6.8, 100 mM NaCl, 300 mM sucrose, 3 mM MgCl<sub>2</sub>, 1 mM EGTA, 1 mM EDTA, 0.5% Triton X-100, 1 mM Pefablock, and 1 mM NaF), and chromatin was solubilized by DNA digestion with 20 U DNase I (New England Biolabs) for 15 min at 37°C. Proteins were extracted by addition of 50  $\mu$ l of 1 M ammonium sulfate to a final concentration of 200 mM, and

samples were pelleted again after 5 min on ice. Soluble chromatin fraction was collected, and the pellet was further extracted with 250  $\mu$ l of 2 M NaCl in cytoplasmic lysis buffer for 5 min on ice and then centrifuged. This treatment removed DNA and histones from the nucleus and the supernatant was collected as a 2 M salt wash fraction. The remaining pellet was solubilized in 250  $\mu$ l of 8 M urea, 0.1 M NaH<sub>2</sub>PO<sub>4</sub>, and 10 mM Tris, pH 8, and considered as a nuclear matrix-containing fraction. The chromatin, 2 M salt wash, and nuclear matrix fractions were diluted two times and analyzed by immunoblot along with the collected cytoplasmic fraction.

### mRNA expression analysis

BjHtERT fibroblasts were transfected with 12 nM TMF-1 siRNA mix or 12 nM nontargeting negative control siRNA (Origene). After 48 h of transfection, cells were serum starved overnight and stimulated or not with 20 ng/ml PDGF-BB for 1 h and 3 h. Cells were lysed, and RNA was prepared with the NucleoSpin RNA Plus kit (Macherey Nagel) according to the manufacturer's instructions. cDNA was prepared from 1  $\mu$ g RNA using the PCR Biosystems cDNA kit, diluted five times, and used for quantitative PCR with the following primers: *HPRT* forward 5'-CCTGGC GTCGTGATTAGTGAT-3', *HPRT* reverse 5'-AGACGTTAGTCCTG TCCATAA-3', *CDKN1A* forward 5'-TGTGAGCAGCTGCCGAAG TCA-3', *CDKN1A* reverse 5'-TGACATGGCGCCTCCTCTGAGT-3', *C-FOS* forward 5'-CGGGGATAGCCTCTCTTACT-3', *C-FOS* reverse 5'-CCAGGTCCGTGCAGAAGTC-3', *NUR77* forward 5'-CTCTGG AGGTCATCCGCAAG-3', *NUR77* reverse 5'-CTGGCTTAGACCTGT ACGCC-3', *AR* forward 5'-GACGACCAGATGGCTGTCATT-3', *AR* reverse 5'-GGGCGAAGTAGAGCATCCTG-3', *PDGFR $\beta$*  forward 5'-AGCACACTGCGTCTGCAGCA-3', and *PDGFR $\beta$*  reverse 5'-TGA GCACCACCAGGGCCAG-3'. The expression levels were calculated as the difference between the cycle threshold value for the control gene and the cycle threshold value of the test gene, taken to the power of 2. Expression levels of tested genes and the level of the TMF-1 knockdown were plotted as the mean of four biological replicates; standard deviation is indicated. *T* test statistical analysis was performed for the difference between mRNA expression levels of *CDKN1A* in control cells versus siTMF knockdown cells.

### Proliferation assay

BjHtERT fibroblasts were seeded in triplicates in a 48-well plate (5,000 cells per well) 3 d after the transfection with Fer, TMF-1, or Brg-1 siRNAs and allowed to attach overnight. The media were replaced with 0.1% FBS in DMEM with increasing concentrations of PDGF-BB up to 20 ng/ml. Full-growth media (10% FBS in DMEM) was used as a control. On day 3 of incubation with PDGF-BB, cells were washed, frozen, and assayed with the CyQuant Cell Proliferation kit (ThermoScientific) as described by the manufacturer. The amount of DNA-incorporated fluorescent dye reflecting the number of cells was analyzed by measuring fluorescence at 480/520 nm with the EnSpire Multimode Reader (Perkin Elmer).

### Online supplemental material

Fig. S1 contains controls for the purity of the nuclear extracts. Validation of nuclear traffic of PDGFR is presented in Fig. S2, as detected separately by two types of PDGFR antibodies used for



costaining in Fig. 1 d. The generality of PDGFR nuclear traffic was confirmed for primary fibroblasts AG1523 and cancer cell lines glioblastoma U105MG and osteosarcoma U2OS, as presented in Fig. S3.

## Acknowledgments

We thank Petter Ranefall from the SciLife BioImage Informatics Facility for creating automatic pipelines for quantification of immunofluorescence images and Maria Tsioumpkou for helpful discussions.

This work was supported by the Ludwig Institute for Cancer Research, the Swedish Cancer Society (grants 2016/445 and 140332), and the Swedish Research Council (grant 2015-02757).

The authors declare no competing financial interests.

Author contributions: N. Papadopoulos designed and performed the experiments and wrote the manuscript. J. Lennartsson and C.-H. Heldin supervised the work and corrected the manuscript.

Submitted: 20 June 2017

Revised: 5 January 2018

Accepted: 1 February 2018

## References

Abraham, G., M. Volpe, S. Shpungin, and U. Nir. 2009. TMF/ARA160 down-regulates proangiogenic genes and attenuates the progression of PC3 xenografts. *Int. J. Cancer*. 125:43–53. <https://doi.org/10.1002/ijc.24277>

Aleksic, T., M.M. Chitnis, O.V. Perestenko, S. Gao, P.H. Thomas, G.D. Turner, A.S. Protheroe, M. Howarth, and V.M. Macaulay. 2010. Type 1 insulin-like growth factor receptor translocates to the nucleus of human tumor cells. *Cancer Res.* 70:6412–6419. <https://doi.org/10.1158/0008-5472.CAN-10-0052>

Berezney, R., M.J. Mortillaro, H. Ma, X. Wei, and J. Samarabandu. 1995. The nuclear matrix: a structural milieu for genomic function. *Int. Rev. Cytol.* 162A:1–65.

Bian, X.-L., H.-Z. Chen, P.-B. Yang, Y.-P. Li, F.-N. Zhang, J.-Y. Zhang, W.-J. Wang, W.-X. Zhao, S. Zhang, Q.-T. Chen, et al. 2017. Nur77 suppresses hepatocellular carcinoma via switching glucose metabolism toward gluconeogenesis through attenuating phosphoenolpyruvate carboxykinase sumoylation. *Nat. Commun.* 8:14420. <https://doi.org/10.1038/ncomms14420>

Boulikas, T. 1995. Chromatin domains and prediction of MAR sequences. *Int. Rev. Cytol.* 162A:279–388.

Carpenter, G., and H.-J. Liao. 2013. Receptor tyrosine kinases in the nucleus. *Cold Spring Harb. Perspect. Biol.* 5:a008979. <https://doi.org/10.1101/cshperspect.a008979>

Carpenter, A.E., T.R. Jones, M.R. Lamprecht, C. Clarke, I.H. Kang, O. Friman, D.A. Guertin, J.H. Chang, R.A. Lindquist, J. Moffat, et al. 2006. Cell-Profiler: image analysis software for identifying and quantifying cell phenotypes. *Genome Biol.* 7:R100. <https://doi.org/10.1186/gb-2006-7-10-r100>

Choudhary, C., J.V. Olsen, C. Brandts, J. Cox, P.N.G. Reddy, F.D. Böhmer, V. Gerke, D.-E. Schmidt-Arras, W.E. Berdel, C. Müller-Tidow, et al. 2009. Mislocalized activation of oncogenic RTKs switches downstream signaling outcomes. *Mol. Cell.* 36:326–339. <https://doi.org/10.1016/j.molcel.2009.09.019>

De Angelis Campos, A.C., M.A. Rodrigues, C. de Andrade, A.M. de Goes, M.H. Nathanson, and D.A. Gomes. 2011. Epidermal growth factor receptors destined for the nucleus are internalized via a clathrin-dependent pathway. *Biochem. Biophys. Res. Commun.* 412:341–346. <https://doi.org/10.1016/j.bbrc.2011.07.100>

Eger, G., N. Papadopoulos, J. Lennartsson, and C.-H. Heldin. 2014. NR4A1 promotes PDGF-BB-induced cell colony formation in soft agar. *PLoS One*. 9:e109047. <https://doi.org/10.1371/journal.pone.0109047>

Euskirchen, G.M., R.K. Auerbach, E. Davidov, T.A. Gianoulis, G. Zhong, J. Rozowsky, N. Bhardwaj, M.B. Gerstein, and M. Snyder. 2011. Diverse roles and interactions of the SWI/SNF chromatin remodeling complex revealed using global approaches. *PLoS Genet.* 7:e1002008. <https://doi.org/10.1371/journal.pgen.1002008>

Forrester, W.C., C. van Genderen, T. Jenuwein, and R. Grosschedl. 1994. Dependence of enhancer-mediated transcription of the immunoglobulin mu gene on nuclear matrix attachment regions. *Science*. 265:1221–1225. <https://doi.org/10.1126/science.8066460>

Fowler, T., R. Sen, and A.L. Roy. 2011. Regulation of primary response genes. *Mol. Cell.* 44:348–360. <https://doi.org/10.1016/j.molcel.2011.09.014>

Fridmann-Sirkis, Y., S. Siniosoglou, and H.R.B. Pelham. 2004. TMF is a golgin that binds Rab6 and influences Golgi morphology. *BMC Cell Biol.* 5:18. <https://doi.org/10.1186/1471-2121-5-18>

Garcia, J.A., S.H. Ou, F. Wu, A.J. Lusis, R.S. Sparkes, and R.B. Gaynor. 1992. Cloning and chromosomal mapping of a human immunodeficiency virus 1 “TATA” element modulatory factor. *Proc. Natl. Acad. Sci. USA*. 89:9372–9376. <https://doi.org/10.1073/pnas.89.20.9372>

Giri, D.K., M. Ali-Seyed, L.-Y. Li, D.-F. Lee, P. Ling, G. Bartholomeusz, S.-C. Wang, and M.-C. Hung. 2005. Endosomal transport of ErbB-2: mechanism for nuclear entry of the cell surface receptor. *Mol. Cell Biol.* 25:11005–11018. <https://doi.org/10.1128/MCB.25.24.11005-11018.2005>

Gomes, D.A., M.A. Rodrigues, M.F. Leite, M.V. Gomez, P. Varnai, T. Balla, A.M. Bennett, and M.H. Nathanson. 2008. c-Met must translocate to the nucleus to initiate calcium signals. *J. Biol. Chem.* 283:4344–4351. <https://doi.org/10.1074/jbc.M706550200>

Guan, B., T.-L. Wang, and I.M. Shih. 2011. ARID1A, a factor that promotes formation of SWI/SNF-mediated chromatin remodeling, is a tumor suppressor in gynecologic cancers. *Cancer Res.* 71:6718–6727. <https://doi.org/10.1158/0008-5472.CAN-11-1562>

Haglund, K., S. Sigismund, S. Polo, I. Szymkiewicz, P.P. Di Fiore, and I. Dikic. 2003. Multiple monoubiquitination of RTKs is sufficient for their endocytosis and degradation. *Nat. Cell Biol.* 5:461–466. <https://doi.org/10.1038/ncb983>

Hao, Q.L., D.K. Ferris, G. White, N. Heisterkamp, and J. Groffen. 1991. Nuclear and cytoplasmic location of the FER tyrosine kinase. *Mol. Cell Biol.* 11:1180–1183. <https://doi.org/10.1128/MCB.11.2.1180>

Heldin, C.H., and B. Westermark. 1999. Mechanism of action and in vivo role of platelet-derived growth factor. *Physiol. Rev.* 79:1283–1316. <https://doi.org/10.1152/physrev.1999.79.4.1283>

Heldin, C.-H., J. Lennartsson, and B. Westermark. 2018. Involvement of platelet-derived growth factor ligands and receptors in tumorigenesis. *J. Intern. Med.* 283:16–44. <https://doi.org/10.1111/joim.12690>

Hsiao, P.W., and C. Chang. 1999. Isolation and characterization of ARA160 as the first androgen receptor N-terminal-associated coactivator in human prostate cells. *J. Biol. Chem.* 274:22373–22379. <https://doi.org/10.1074/jbc.274.32.22373>

Jackson, D.A., A.B. Hassan, R.J. Errington, and P.R. Cook. 1993. Visualization of focal sites of transcription within human nuclei. *EMBO J.* 12:1059–1065.

Kadoch, C., D.C. Hargreaves, C. Hodges, L. Elias, L. Ho, J. Ranish, and G.R. Crabtree. 2013. Proteomic and bioinformatic analysis of mammalian SWI/SNF complexes identifies extensive roles in human malignancy. *Nat. Genet.* 45:592–601. <https://doi.org/10.1038/ng.2628>

Kapeller, R., R. Chakrabarti, L. Cantley, F. Fay, and S. Corvera. 1993. Internalization of activated platelet-derived growth factor receptor-phosphatidylinositol-3' kinase complexes: potential interactions with the microtubule cytoskeleton. *Mol. Cell Biol.* 13:6052–6063. <https://doi.org/10.1128/MCB.13.10.6052>

Kermorgant, S., and P.J. Parker. 2008. Receptor trafficking controls weak signal delivery: a strategy used by c-Met for STAT3 nuclear accumulation. *J. Cell Biol.* 182:855–863. <https://doi.org/10.1083/jcb.200806076>

Kimura, M., and N. Imamoto. 2014. Biological significance of the importin-β family-dependent nucleocytoplasmic transport pathways. *Traffic.* 15:727–748. <https://doi.org/10.1111/tra.12174>

Laemmli, U.K., E. Käs, L. Poljak, and Y. Adachi. 1992. Scaffold-associated regions: cis-acting determinants of chromatin structural loops and functional domains. *Curr. Opin. Genet. Dev.* 2:275–285. [https://doi.org/10.1016/S0959-437X\(05\)80285-0](https://doi.org/10.1016/S0959-437X(05)80285-0)

Lemmon, M.A., and J. Schlessinger. 2010. Cell signaling by receptor tyrosine kinases. *Cell.* 141:1117–1134. <https://doi.org/10.1016/j.cell.2010.06.011>

Lennartsson, J., H. Ma, P. Wardega, K. Pelka, U. Engström, C. Hellberg, and C.-H. Heldin. 2013. The Fer tyrosine kinase is important for platelet-derived growth factor-BB-induced signal transducer and activator of transcription 3 (STAT3) protein phosphorylation, colony formation in soft



- agar, and tumor growth in vivo. *J. Biol. Chem.* 288:15736–15744. <https://doi.org/10.1074/jbc.M113.476424>
- Li, L.-Y., H. Chen, Y.-H. Hsieh, Y.-N. Wang, H.-J. Chu, Y.-H. Chen, H.-Y. Chen, P.-J. Chien, H.-T. Ma, H.-C. Tsai, et al. 2011. Nuclear ErbB2 enhances translation and cell growth by activating transcription of ribosomal RNA genes. *Cancer Res.* 71:4269–4279. <https://doi.org/10.1158/0008-5472.CAN-10-3504>
- Lin, S.Y., K. Makino, W. Xia, A. Matin, Y. Wen, K.Y. Kwong, L. Bourguignon, and M.C. Hung. 2001. Nuclear localization of EGF receptor and its potential new role as a transcription factor. *Nat. Cell Biol.* 3:802–808. <https://doi.org/10.1038/ncb0901-802>
- Liu, P., Y. Ying, Y.G. Ko, and R.G. Anderson. 1996. Localization of platelet-derived growth factor-stimulated phosphorylation cascade to caveolae. *J. Biol. Chem.* 271:10299–10303. <https://doi.org/10.1074/jbc.271.17.10299>
- Lo, H.-W., M. Ali-Seyed, Y. Wu, G. Bartholomeusz, S.-C. Hsu, and M.-C. Hung. 2006. Nuclear-cytoplasmic transport of EGFR involves receptor endocytosis, importin beta and CRM1. *J. Cell. Biochem.* 98:1570–1583. <https://doi.org/10.1002/jcb.20876>
- Miaczynska, M. 2013. Effects of membrane trafficking on signaling by receptor tyrosine kinases. *Cold Spring Harb. Perspect. Biol.* 5:a009035. <https://doi.org/10.1101/cshperspect.a009035>
- Miaczynska, M., L. Pelkmans, and M. Zerial. 2004. Not just a sink: endosomes in control of signal transduction. *Curr. Opin. Cell Biol.* 16:400–406. <https://doi.org/10.1016/j.cob.2004.06.005>
- Miller, V.J., P. Sharma, T.A. Kudlyk, L. Frost, A.P. Rofe, I.J. Watson, R. Duden, M. Lowe, V.V. Lupashin, and D. Ungar. 2013. Molecular insights into vesicle tethering at the Golgi by the conserved oligomeric Golgi (COG) complex and the golgin TATA element modulatory factor (TMF). *J. Biol. Chem.* 288:4229–4240. <https://doi.org/10.1074/jbc.M112.426767>
- Mori, K., and H. Kato. 2002. A putative nuclear receptor coactivator (TMF/ARA160) associates with hbrm/hSNF2 alpha and BRG-1/hSNF2 beta and localizes in the Golgi apparatus. *FEBS Lett.* 520:127–132. [https://doi.org/10.1016/S0014-5793\(02\)02803-X](https://doi.org/10.1016/S0014-5793(02)02803-X)
- Mori, S., C.H. Heldin, and L. Claesson-Welsh. 1992. Ligand-induced polyubiquitination of the platelet-derived growth factor beta-receptor. *J. Biol. Chem.* 267:6429–6434.
- Nakayama, Y., A. Kawana, A. Igarashi, and N. Yamaguchi. 2006. Involvement of the N-terminal unique domain of Chk tyrosine kinase in Chk-induced tyrosine phosphorylation in the nucleus. *Exp. Cell Res.* 312:2252–2263. <https://doi.org/10.1016/j.yexcr.2006.03.021>
- Packham, S., D. Warsito, Y. Lin, S. Sadi, R. Karlsson, B. Sehat, and O. Larsson. 2015. Nuclear translocation of IGF-1R via p150(Glued) and an importin-β/RanBP2-dependent pathway in cancer cells. *Oncogene.* 34:2227–2238. <https://doi.org/10.1038/ncr.2014.165>
- Papadopoulos, N., and J. Lennartsson. 2017. The PDGF/PDGFR pathway as a drug target. *Mol. Aspects Med.* S0098-2997(17)30140-1. <https://doi.org/10.1016/j.mam.2017.11.007>
- Perry, E., R. Tsruya, P. Levitsky, O. Pomp, M. Tallar, S. Weisberg, W. Parris, S. Kulkarni, H. Malovani, T. Pawson, et al. 2004. TMF/ARA160 is a BC-box-containing protein that mediates the degradation of Stat3. *Oncogene.* 23:8908–8919. <https://doi.org/10.1038/sj.onc.1208149>
- Radha, V., S. Nambirajan, and G. Swarup. 1996. Association of Lyn tyrosine kinase with the nuclear matrix and cell-cycle-dependent changes in matrix-associated tyrosine kinase activity. *Eur. J. Biochem.* 236:352–359. <https://doi.org/10.1111/j.1432-1033.1996.00352.x>
- Ramirez-Carrozzi, V.R., D. Braas, D.M. Bhatt, C.S. Cheng, C. Hong, K.R. Doty, J.C. Black, A. Hoffmann, M. Carey, and S.T. Smale. 2009. A unifying model for the selective regulation of inducible transcription by CpG islands and nucleosome remodeling. *Cell.* 138:114–128. <https://doi.org/10.1016/j.cell.2009.04.020>
- Rando, O.J., K. Zhao, P. Janmey, and G.R. Crabtree. 2002. Phosphatidylinositol-dependent actin filament binding by the SWI/SNF-like BAF chromatin remodeling complex. *Proc. Natl. Acad. Sci. USA.* 99:2824–2829. <https://doi.org/10.1073/pnas.032662899>
- Reyes, J.C., C. Muchardt, and M. Yaniv. 1997. Components of the human SWI/SNF complex are enriched in active chromatin and are associated with the nuclear matrix. *J. Cell Biol.* 137:263–274. <https://doi.org/10.1083/jcb.137.2.263>
- Schlessinger, J., and M.A. Lemmon. 2006. Nuclear signaling by receptor tyrosine kinases: the first robin of spring. *Cell.* 127:45–48. <https://doi.org/10.1016/j.cell.2006.09.013>
- Schwartz, Y., I. Ben-Dor, A. Navon, B. Motro, and U. Nir. 1998. Tyrosine phosphorylation of the TATA element modulatory factor by the FER nuclear tyrosine kinases. *FEBS Lett.* 434:339–345. [https://doi.org/10.1016/S0014-5793\(98\)01003-5](https://doi.org/10.1016/S0014-5793(98)01003-5)
- Sehat, B., A. Tofigh, Y. Lin, E. Trocmé, U. Liljedahl, J. Lagergren, and O. Larsson. 2010. SUMOylation mediates the nuclear translocation and signaling of the IGF-1 receptor. *Sci. Signal.* 3:ra10. <https://doi.org/10.1126/scisignal.2000628>
- Sigmund, S., E. Argenzio, D. Tosoni, E. Cavallaro, S. Polo, and P.P. Di Fiore. 2008. Clathrin-mediated internalization is essential for sustained EGFR signaling but dispensable for degradation. *Dev. Cell.* 15:209–219. <https://doi.org/10.1016/j.devcel.2008.06.012>
- Simone, C. 2006. SWI/SNF: the crossroads where extracellular signaling pathways meet chromatin. *J. Cell. Physiol.* 207:309–314. <https://doi.org/10.1002/jcp.20514>
- Sorkin, A., B. Westermark, C.H. Heldin, and L. Claesson-Welsh. 1991. Effect of receptor kinase inactivation on the rate of internalization and degradation of PDGF and the PDGF beta-receptor. *J. Cell Biol.* 112:469–478. <https://doi.org/10.1083/jcb.112.3.469>
- Stachowiak, M.K., P.A. Maher, A. Joy, E. Mordechai, and E.K. Stachowiak. 1996a. Nuclear localization of functional FGF receptor 1 in human astrocytes suggests a novel mechanism for growth factor action. *Brain Res. Mol. Brain Res.* 38:161–165. [https://doi.org/10.1016/0169-328X\(96\)00010-1](https://doi.org/10.1016/0169-328X(96)00010-1)
- Stachowiak, M.K., P.A. Maher, A. Joy, E. Mordechai, and E.K. Stachowiak. 1996b. Nuclear accumulation of fibroblast growth factor receptors is regulated by multiple signals in adrenal medullary cells. *Mol. Biol. Cell.* 7:1299–1317. <https://doi.org/10.1091/mbc.7.8.1299>
- Stachowiak, M.K., P.A. Maher, and E.K. Stachowiak. 2007. Integrative nuclear signaling in cell development—a role for FGF receptor-1. *DNA Cell Biol.* 26:811–826. <https://doi.org/10.1089/dna.2007.0664>
- Strouboulis, J., and A.P. Wolffe. 1996. Functional compartmentalization of the nucleus. *J. Cell Sci.* 109:1991–2000.
- Volpe, M., S. Shpungin, C. Barbi, G. Ahrham, H. Malovani, R. Wides, and U. Nir. 2006. trnp: A conserved mammalian gene encoding a nuclear protein that accelerates cell-cycle progression. *DNA Cell Biol.* 25:331–339. <https://doi.org/10.1089/dna.2006.25.331>
- Wang, S.-C., Y. Nakajima, Y.-L. Yu, W. Xia, C.-T. Chen, C.-C. Yang, E.W. McIntush, L.-Y. Li, D.H. Hawke, R. Kobayashi, and M.-C. Hung. 2006. Tyrosine phosphorylation controls PCNA function through protein stability. *Nat. Cell Biol.* 8:1359–1368. <https://doi.org/10.1038/ncb1501>
- Wang, Y.-N., H. Wang, H. Yamaguchi, H.-J. Lee, H.-H. Lee, and M.-C. Hung. 2010a. COPI-mediated retrograde trafficking from the Golgi to the ER regulates EGFR nuclear transport. *Biochem. Biophys. Res. Commun.* 399:498–504. <https://doi.org/10.1016/j.bbrc.2010.07.096>
- Wang, Y.-N., H. Yamaguchi, J.-M. Hsu, and M.-C. Hung. 2010b. Nuclear trafficking of the epidermal growth factor receptor family membrane proteins. *Oncogene.* 29:3997–4006. <https://doi.org/10.1038/ncr.2010.157>
- Wang, Y.-N., H. Yamaguchi, L. Huo, Y. Du, H.-J. Lee, H.-H. Lee, H. Wang, J.-M. Hsu, and M.-C. Hung. 2010c. The translocon Sec1beta localized in the inner nuclear membrane transports membrane-embedded EGF receptor to the nucleus. *J. Biol. Chem.* 285:38720–38729. <https://doi.org/10.1074/jbc.M110.158659>
- Wang, Y.-N., H.-H. Lee, H.-J. Lee, Y. Du, H. Yamaguchi, and M.-C. Hung. 2012. Membrane-bound trafficking regulates nuclear transport of integral epidermal growth factor receptor (EGFR) and ErbB-2. *J. Biol. Chem.* 287:16869–16879. <https://doi.org/10.1074/jbc.M111.314799>
- Warsito, D., Y. Lin, A.-C. Gnirck, B. Sehat, and O. Larsson. 2016. Nuclearly translocated insulin-like growth factor 1 receptor phosphorylates histone H3 at tyrosine 41 and induces SNAI2 expression via Brg1 chromatin remodeling protein. *Oncotarget.* 7:42288–42302. <https://doi.org/10.18632/oncotarget.9785>
- Wilson, B.G., and C.W.M. Roberts. 2011. SWI/SNF nucleosome remodellers and cancer. *Nat. Rev. Cancer.* 11:481–492. <https://doi.org/10.1038/nrc3068>
- Wong, M., and S. Munro. 2014. Membrane trafficking. The specificity of vesicle traffic to the Golgi is encoded in the golgin coiled-coil proteins. *Science.* 346:1256898. <https://doi.org/10.1126/science.1256898>
- Yamane, J., A. Kubo, K. Nakayama, A. Yuba-Kubo, T. Katsuno, S. Tsukita, and S. Tsukita. 2007. Functional involvement of TMF/ARA160 in Rab6-dependent retrograde membrane traffic. *Exp. Cell Res.* 313:3472–3485. <https://doi.org/10.1016/j.yexcr.2007.07.010>
- Yu, J., X.-W. Liu, and H.-R.C. Kim. 2003. Platelet-derived growth factor (PDGF) receptor-alpha-activated c-Jun NH2-terminal kinase-1 is critical for PDGF-induced p21WAF1/CIP1 promoter activity independent of p53. *J. Biol. Chem.* 278:49582–49588. <https://doi.org/10.1074/jbc.M309986200>
- Zhao, K., W. Wang, O.J. Rando, Y. Xue, K. Swiderek, A. Kuo, and G.R. Crabtree. 1998. Rapid and phosphoinositide-dependent binding of the SWI/SNF-like BAF complex to chromatin after T lymphocyte receptor signaling. *Cell.* 95:625–636. [https://doi.org/10.1016/S0092-8674\(00\)81633-5](https://doi.org/10.1016/S0092-8674(00)81633-5)